A Fresh Look at Practical Shunt Reactor Protection

Ritwik Chowdhury and Normann Fischer
Schweitzer Engineering Laboratories, Inc.

Douglas Taylor
Avista Utilities

David Caverly
Trench Limited

Ali B. Dehkordi
RTDS Technologies Inc.

Revised edition released October 2022

Originally presented at the
49th Annual Western Protective Relay Conference, October 2022

A Fresh Look at Practical Shunt Reactor Protection

Ritwik Chowdhury and Normann Fischer, *Schweitzer Engineering Laboratories, Inc.*
Douglas Taylor, *Avista Utilities*
David Caverly, *Trench Limited*
Ali B. Dehkordi, *RTDS Technologies Inc.*

***Abstract*—Most reactor faults begin as low-grade turn-to-turn faults (i.e., with one turn or very few turns shorted) and, when undetected and uncleared, may involve more turns or evolve into phase-to-ground faults or even phase-to-phase faults. Detecting and clearing a reactor fault quickly is essential in limiting damage, especially in oil-immersed reactors with possible fire hazards.**

This paper evaluates the limits of shunt reactor protection by considering the magnetic and physical characteristic differences between air-core and iron-core reactors. For turn-to-turn faults in air-core reactors, the magnetic flux generated by the faulted turns may only partially couple with the healthy turns. In contrast, the core in iron-core reactors substantially couples the magnetic flux between the faulted turns and the healthy turns. Because of the lower coupling in air-core reactors versus iron-core reactors, the fault current is reduced, which consequently lowers protection sensitivity. On the other hand, the saturation characteristics of an iron-core reactor result in inrush currents that have sequence quantities, which impact protection security.

For turn-to-turn fault protection, the paper discusses the use of, and presents settings guidelines for, a new scheme using directional sequence overcurrent elements. Due to the large number of turns in an extra-high-voltage (EHV) reactor, it may not be possible to detect faults involving a single turn. However, the paper presents equations and tools that approximate the percentage of shorted turns that can be detected. Based on the reactor model and protection scheme settings, turn-to-turn faults can be cleared within a few cycles with sensitivities of around 0.1% for iron-core reactors and 0.2% for air-core reactors. The paper provides CT selection criteria, primarily driven by the sensitivity requirements for turn-to-turn faults. Settings guidelines to ensure protection security during reactor energization are also provided. A novel method for protection security during line de-energization is presented. The use of special timers to improve dependability for intermittent ground faults on an ungrounded transformer tertiary bus connected reactor is also discussed.

The paper uses a new electromagnetic transient (EMT) model and field events of reactor inrush and turn-to-turn faults to demonstrate the security and dependability of the protection schemes discussed. These schemes are comprehensive, providing optimal protection for phase-to-phase, phase-to-ground, and turn-to-turn faults for different reactor applications. They have been applied to protect an air-core reactor at a utility, Avista, with great field experience.

I. Introduction

Shunt reactors aid voltage control in power systems. The common applications of shunt reactors are shown in Fig. 1 [1] [2]. Transmission or distribution bus-connected shunt reactors (Fig. 1a) are typically solidly grounded. Reactors on the transformer tertiary bus (Fig. 1c) are typically ungrounded and provide a convenient place to provide voltage regulation. Line-connected shunt reactors (Fig. 1b) typically compensate 70% to 80% of the capacitive charging current in long lines [3] to mitigate overvoltages during light loads. In single-phase tripping applications, a four-reactor bank may be used with a neutral (fourth) reactor to aid secondary arc-extinction [3].

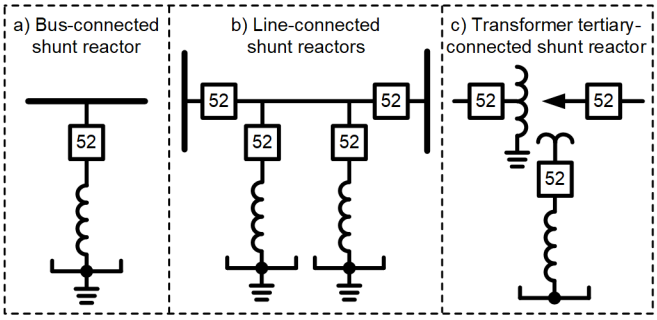

Fig. 1. Typical shunt reactor applications and connections [1].

There are two types of reactors—air-core and gapped iron-core. Typically, air-core reactors are dry-type (see Fig. 2) and iron-core reactors are oil-immersed in a tank (see Fig. 3). In the distant past, air-core reactors were applied at medium-voltage (MV) levels of 34.5 kV or lower [4]. However, improvements in technology have allowed manufacturing of air-core reactors for extra-high-voltage (EHV) applications, with ratings up to 800 kV or higher and 600 MVAR (60 Hz equivalent) for series applications [1] [5], and up to 550 kV and 200 MVAR for shunt reactors [6].

EHV air-core reactor banks at Avista were applied to address environmental concerns near the Clark Fork River; one of these banks is shown in Fig. 2. Each reactor phase has four coils—there are two stacks with two coils each. A simplified assumption we make in this paper is that the coils in a stack magnetically couple, whereas there is minimal coupling between two stacks.

Fig. 2. A three-phase dry-type air-core shunt reactor (238 kV, 50 MVAR).

Fig. 3. An oil-immersed iron-core shunt reactor.

The paper is organized as follows—Section II introduces the concepts that challenge protection security and impact turn-to-turn (or simply, turn) fault sensitivity. Section III provides an overview of the primary protection elements considered for shunt reactor protection. Section IV presents an improved turn fault protection scheme, dependability enhancement to an existing ground fault protection scheme, and detailed settings guidelines for phase, ground, and turn fault protection based on security. Field events and simulations are used to demonstrate protection security. Section V shows the use of a new model for a real-time digital simulator (RTDS) model and field events of turn faults from Xcel Energy [7] to illustrate protection dependability, including sensitivity and speed. The turn fault protection sensitivity is shown to be around 0.1% for iron-core reactors and 0.2% for air-core reactors with speed limited by intentional security delays of 1.5 to 3 cycles. The paper shares a new model and the associated MATLAB and Mathcad tools in Appendix A to help approximate turn fault currents, allowing evaluation of the sensitivity provided by turn fault protection elements. Appendix B shares the protection and targeting settings deployed at Avista to protect their reactor.

II. Reactor Bank Protection Considerations

A. Shunt Reactor Fault Types

The different reactor fault types are shown in Fig. 4.

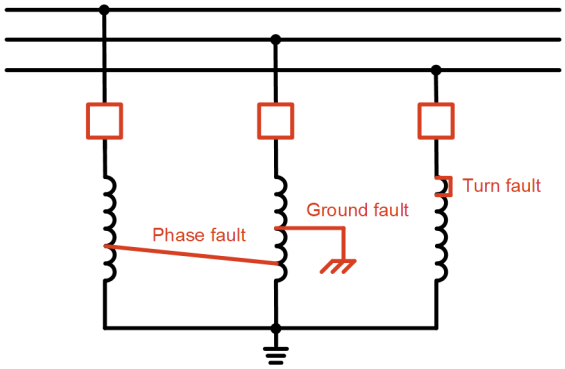

Fig. 4. Fault types in a shunt reactor.

Air-core reactor phases are separated in space significantly and have adequate insulation to ground; therefore, the likelihood of phase and ground faults is low. Iron-core reactors are oil-immersed and face a greater likelihood of a ground or a phase fault due to the proximity of the core to the tank and the proximity of the phase windings to one another, respectively [1]. Turn faults can occur in both air-core reactors and iron-core reactors. In air-core reactors, because of the low probability of phase and ground faults, turn faults are by far the most likely fault type.

B. Security Considerations

1) Reactor Unbalance

IEEE Std C57.21-2021 requires that "the maximum deviation of impedance in any one phase shall be within ±2% of the average impedance of the three phases" [8]. An example of the worst-case unbalance is when the three phases have impedances of 0.98 pu, 1 pu, and 1.02 pu, respectively. This unbalance translates to a negative-sequence current (I2) value of 1.15% or a 3I2 value of 3.46%; the same values apply to zero-sequence current (I0) in a solidly grounded reactor bank. This places a limit on how sensitively shunt reactor protection can be set.

2) Reactor Inrush

Iron-core reactors have a nonlinear core, which results in the saturation characteristic shown in Fig. 5. Based on data sheets of iron-core reactors deployed in the field, they can be designed to be linear up to 150% of their rated voltage (within a specified tolerance of 5% [9]), although they may be sized to be linear to lower values (e.g., 130%) to reduce cost. Their inrush current levels (in per-unit) are lower than the inrush current levels of power transformers, because the gap in the iron-core limits residual flux.

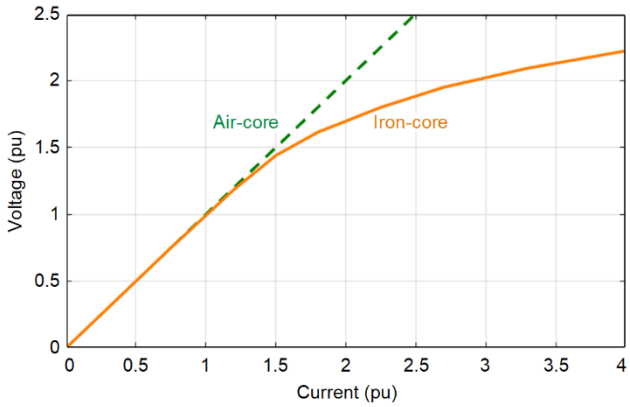

Fig. 5. Voltage vs. current for air-core and gapped iron-core reactors.

The saturation of an iron-core reactor creates an unbalance, which adds I0 and I2 to inrush currents (see Fig. 6). An air-core reactor has a linear saturation characteristic, resulting in no I0 or I2 during inrush except for a measurement filter transient for I2. We use the term "inrush" to describe the transient resulting from reactor energization in accordance with accepted IEEE and IEC definitions—thus, not only the magnetizing inrush current of an iron-core reactor, but also the dc offset current that is dependent on the point-on-wave of energization.

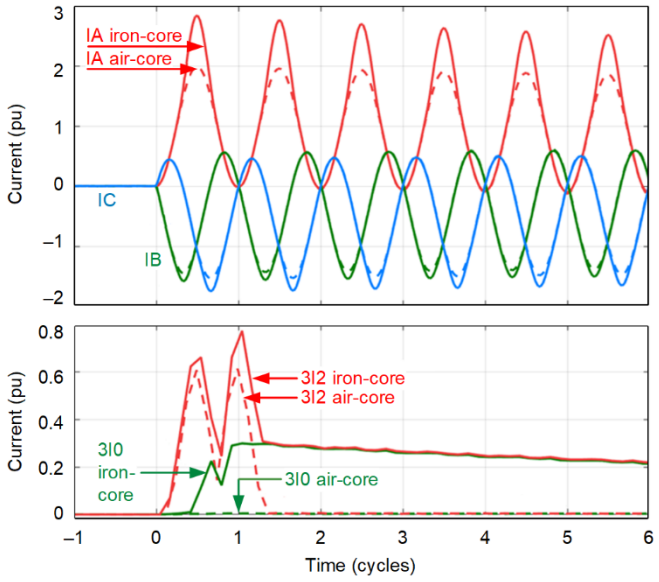

Fig. 6. Comparison of inrush in an iron-core and air-core reactor using a simulation without CT saturation.

The inrush currents of Fig. 6 have dc offsets that decay very slowly because reactors have the highest reactance-to-resistance (X/R) ratios in the power system. An air-core reactor X/R ranges from 300 to 500 [7] with a dc time constant of about 1 second. Iron-core reactors have twice these values. Long-lasting current dc offsets can cause slow CT saturation, which adds additional I0 and I2 during inrush. Additionally, unequal CT saturation can challenge the differential element. We characterize the impact of CT saturation and iron-core reactor saturation on protection in Section IV.

C. *Sensitivity for Reactor Turn Faults*

It may seem that due to the saturation of an iron-core reactor, in addition to the standing unbalance and CT saturation, turn fault protection sensitivity for an iron-core reactor would be lower than an air-core reactor, and it is true that iron-core reactor protection settings would be set less sensitively or have slower operating times. However, the fault currents and measurable terminal currents shorting the same percentage of turns in an iron-core reactor are much higher than those in an air-core reactor, which tips sensitivity in favor of an iron-core reactor. This requires understanding the magnetic circuit and physical structural differences between an iron-core reactor and an air-core reactor.

1) *Magnetic Circuit During Reactor Turn Faults*

The differences between the behavior of magnetic flux in an air-core versus an iron-core reactor are shown in Fig. 7. The many healthy turns and their flux are shown in black, whereas the single faulted turn and its flux are shown in red. The healthy turns contribute a flux that adds to a large main flux that flows through an air-core and an iron-core reactor.

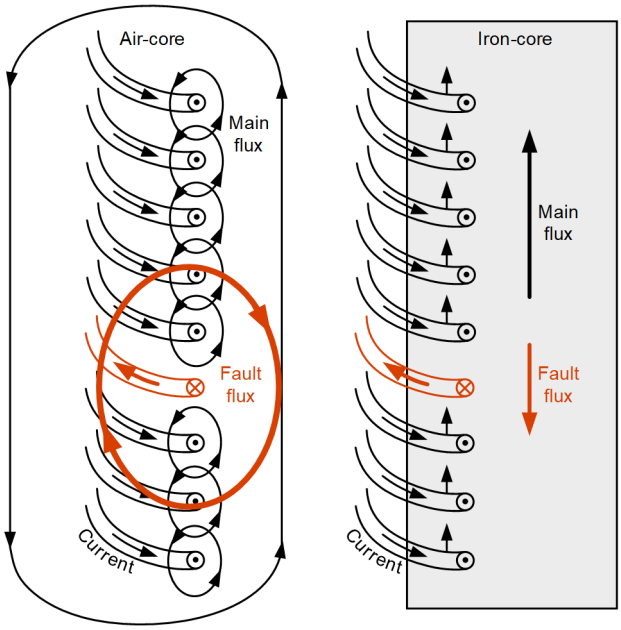

Fig. 7. Comparison of air-core and iron-core reactor flux during a turn fault.

During a turn fault, the current and the magnetic flux generated by the faulted turns are in the opposite direction of the field generated by the healthy turns. This causes the net magnetic flux crossing the shorted portion of the reactor to be zero. The iron-core presents a low-reluctance path that channels the flux throughout the winding and provides more complete coupling. Therefore, most of the total inductance in an iron-core reactor is the mutual inductance, whereas the leakage inductance is small. In magnetic devices, a smaller leakage is generally associated with higher fault currents. Conversely, in air-core reactors, the magnetic flux generated by the faulted turns scatters and attenuates significantly as it gets further away from the faulted turns. This results in lower mutual coupling with the healthy turns of the air-core reactor, which in turn induces a lower current in the healthy turns (as compared to an iron-core reactor).

Based on the above principles, the per-unit faulted turn currents are expected to be higher in an iron-core reactor than in an air-core reactor of the same rating. This is illustrated using the Avista reactor parameters of Table I in Fig. 8, which has two stacks. Fig. 8 is based on the model in Appendix A with the reactor type varied (air-core vs. iron-core) and coil layout (number of stacks) varied.

TABLE I
AVISTA REACTOR AND SYSTEM DATA

Parameter	Value
Reactor type	Dry-type air-core
Coil layout per phase	2 stacks with 2 coils per stack
Radius (r) and height (h) of a coil	4.2 ft (1.28 m) and 11 ft (3.4 m)
Grounding	Solidly grounded
Rated voltage, MVA, and frequency	238 kV, 50 MVAR, and 60 Hz
Rated current (I_{RATED})	121.3 A primary
Potential transformer ratio (PTR)	2000
Phase CT ratio (CTR)	240
Neutral CT ratio (CTRN)	80
Phase CT nominal current (I_{NOM_CTR})	1 A secondary
Neutral CT nominal current (I_{NOM_CTRN})	1 A secondary
Total reactance (X_L)	1,133 Ω primary or 139.9 Ω secondary
System impedance (Z_{SYS})	9.29 Ω primary∠86° (normal) 15.09 Ω primary∠86°(N – 1)

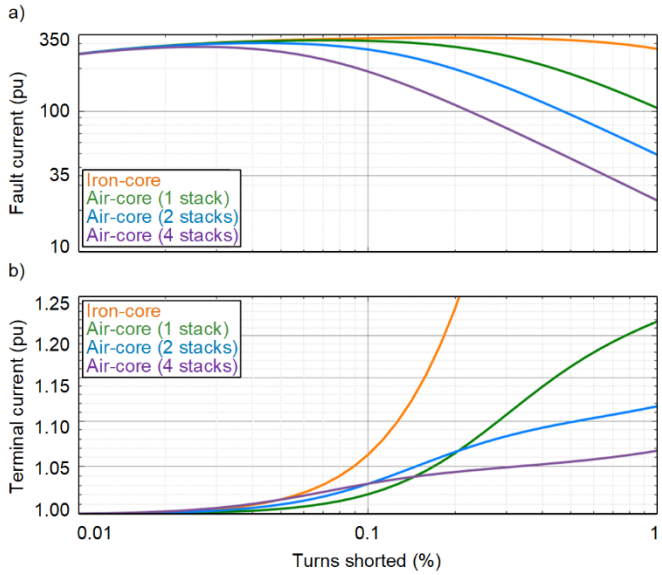

Fig. 8. For turn faults shorting up to 1%, a) large, unmeasured fault currents in the shorted turns and b) small, measured currents at the reactor terminals.

The fault currents in the shorted turns are plotted in Fig. 8a; they can be hundreds of times the rated reactor current and can cause significant damage if not cleared. However, these fault currents circulate within the shorted turns and are unmeasured by the terminal CTs protecting the reactor bank. The measured currents are shown in Fig. 8b. For instance, the measurable current is 6.3% greater than the rated current for a 0.1% turn fault in the iron-core reactor. Whereas, for a 0.2% turn fault in an air-core reactor with one, two, and four stacks, the measurable currents are 6.4%, 6.6%, and 4.4%, respectively. These increased currents manifest as 3I2 and neutral current (IN) measurements, which can then be used for protection.

In Section V, we use a new faulted shunt reactor model in the RTDS simulator for hardware-in-the-loop testing [10]. The model can short 1% to 98% of the reactor turns. This single-phase faulted reactor model allows users to put as many as two fault points on the reactor. This allows for the modeling of phase, ground, and turn faults. The model generates the inductance matrix of the set of mutually coupled inductors based on the reactor type.

In an iron-core reactor, the mutual coupling between the windings couples through an iron path that is ideal or complete; therefore, the inductance values of the inductance matrix are proportional to the square of the number of turns.

In an air-core reactor, the windings are coupled through air, and the amount of coupling depends on the dimensions of the coils, mainly the ratio of the coil radius over the stack height. The model provides the user with a factor (MfacAir) indicating the strength of mutual coupling in the air. This factor is a value between 0.0 and 1.0. A value of 1.0 indicates ideal mutual coupling, and the inductance values of the inductance matrix are proportional to the square of the number of turns. The value of 0.0 indicates no mutual coupling between the windings, and the inductance values of the inductance matrix are proportional to the number of turns. In this case, off-diagonal values of the inductance matrix are 0.0. For a practical air-core reactor, this value is somewhere between 0.0 and 1.0. To precisely determine the value of this factor, the user has to solve the field equations or refer to empiric formulas [11] [12].

The general equations for the faulted shunt reactor model [10] are shown in (1). In this equation, L_{sr} is the total inductance of the shunt reactor, L_m is the magnetizing portion of the inductance, and L_l is the leakage portion of inductance. For an air-core reactor, the total inductance of the reactor is used for L_l, and $L_{iron\text{-}path}$ is eliminated from the equation. The variables n_1 and n_2 are the normalized number of turns for each divided section of the reactor, and their value is between 0.0 and 1.0. This model is different from the simplified model in Appendix A and has different parameters, but, as shown later in Section V, it can produce similar currents.

$$\left[L_{sr}\right]=\left[L_{air\text{-}path}\right]+\left[L_{iron\text{-}path}\right]$$

where:

$$\left[L_{iron\text{-}path}\right]=\begin{bmatrix} n_1^2 & n_1n_2 \\ n_1n_2 & n_2 \end{bmatrix}\bullet L_m$$

$$\left[L_{air\text{-}path}\right]=(1-\alpha)\bullet\begin{bmatrix} n_1 & 0 \\ 0 & n_2 \end{bmatrix}\bullet L_l+(\alpha)\bullet\begin{bmatrix} n_1^2 & n_1n_2 \\ n_1n_2 & n_2^2 \end{bmatrix}\bullet L_l \quad (1)$$

α = MfacAir (factor for mutual coupling in the air)

$$n_1=\frac{N_1}{N} \text{ and } n_2=\frac{N_2}{N}$$

In the past, protection engineers sometimes treated a faulted reactor as an unbalanced reactor to estimate the measured unbalance current [1]. The faulted turns were considered as if they were removed from the circuit, and their fault current and flux were ignored. In Fig. 9, this unbalanced reactor model is compared to the equivalent impedance presented by the faulted air-core and faulted iron-core reactor models of Appendix A. It

is clear that the high fault currents of Fig. 8a induce significant flux, which makes an unbalanced reactor model inaccurate. Both Fig. 8b and Fig. 9 suggest that the reduced impedance presented by the reactor makes it easier to detect a turn fault than assumed in the past.

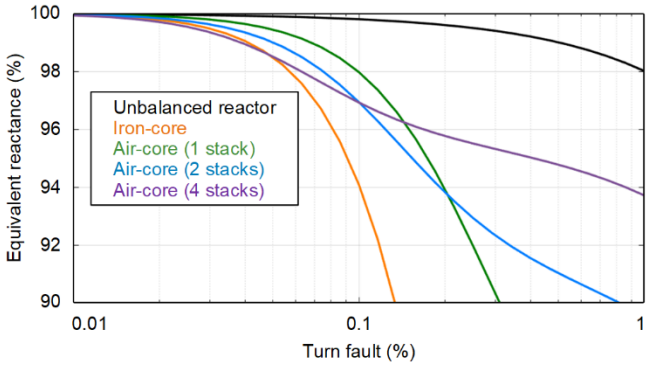

Fig. 9. Faulted winding equivalent reactance due to a turn fault.

2) Reactor Parameters

It may seem that there is adequate current for faults that short less than 1% of a reactor phase, but it is important to recognize that reactors can have up to a few thousand turns. The parameters for several air-core reactors and iron-core reactors are presented in Table II and Table III, respectively. The A and B in Table II refers to newer and older air-core reactor manufacturing technology, respectively, whereas the I in Table III refers to an iron-core reactor.

The Avista reactor of Fig. 2 is the 3B reactor in Table II. It was manufactured in 2015, with a version of what is now older technology, and had nearly 4,000 turns. A single turn fault (~0.025%) in this reactor can induce very large fault currents (~300 pu as shown in Fig. 8a); but as evident from Fig. 8b, this current is not measurable at the reactor terminals. Although initially undetectable, such a fault rapidly melts turn insulation and also melts the winding turns. The fault then rapidly progresses to involve more turns, at which point, it is detectable. Such progression is evident from field events of turn faults from Xcel Energy [7], also shown later in Section V.C.

Air-core reactors may have multiple concentric cylindrical windings or packages, each of which may consist of one or more layers with individual conductors (wires or cables) (see Fig. 10) [5] [13]. The use of multiple packages, layers, and conductors is one way to ensure that the reactor has an adequate current-carrying capability to achieve the desired MVAR rating. The presence of packages and layers and their particular arrangement can also impact turn fault currents (and consequently, protection sensitivity), but their impacts are not considered in this paper. Modern high-voltage (HV) and EHV air-core reactors sometimes have a single package wound with a single layer of cable and may also have fewer turns.

Oil-immersed iron-core reactors have a single layer, fewer turns, and stronger coupling than air-core reactors that helps ensure the availability of higher measurable fault currents for protection. It is also important to clear faults in these reactors quickly due to possible fire and explosion hazards. From this perspective, speed is a more important criterion for oil-immersed iron-core reactor protection (due to the oil), whereas sensitivity is a more important criterion for air-core reactor protection.

With recent advancements in air-core reactor designs, single-package coils are common at HV and EHV voltages. The number of turns in these reactors (see A reactors in Table II) are around twice that of iron-core reactors of similar ratings (see Table III). As a result, although the sensitivity differences are still present, they are less than what a user might expect.

TABLE II
PARAMETERS FOR SEVERAL AIR-CORE SHUNT REACTORS

Para-meter	1A	2A	3B	3A	4A	5A	6A
Voltage (kV)	13.8	34.5	238	238	345	420	500
MVAR	20	50	50	50	120	120	125
Frequency (Hz)	60	60	60	60	60	50	60
Current (A)	837	837	121	121	201	165	144
#Stacks / phase	1	1	2	2	1	2	2
#Coils / stack	1	1	2	2	4	2	3
Radius (in)	60.5	41.3	35.3	66.2	68.1	73.1	68.2
Length (in)	54.4	55.6	455	470	480	621	731
Inductance (mH)	25.3	63	3,005	3,005	2,631	4,679	5,305
Turns / phase	90	207	3,943	2,096	1,834	2,644	3,322

TABLE III
PARAMETERS FOR SEVERAL IRON-CORE SHUNT REACTORS

Parameter	3I	4I	5I	6I
Voltage (kV)	230	345	400	500
MVAR	50	150	150	175
Frequency (Hz)	60	60	50	60
Current (A)	126	251	217	202
Radius (in)	15.8	21.6	23.2	21.7
Active part height (in)	88.0	110.2	110.2	118.1
Winding height (in)	56.7	67.2	59.1	70.9
Inductance (mH)	2,806	2,105	3,395	3,789
Turns / phase	1,982	1,170	1,470	1,570

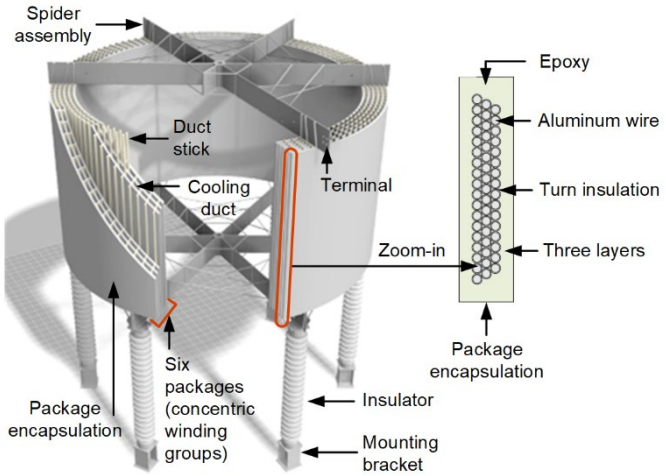

Fig. 10. Dry-type air-core reactor with six packages and three layers.

D. *Reactor Bank Sequence Network*

Turn fault protection elements often rely on I0 or I2, measured by three phase CTs at the reactor terminals, to help detect an internal fault. Therefore, it is helpful to consider the sequence network of Fig. 11 for low-grade turn faults. When a turn fault occurs, an equivalent fault impedance (Z_{FAULT}) connects the three sequence networks at the fault location. The sign of Z_{FAULT} is negative because of the opposite direction of the faulted flux, relative to the main flux (see Fig. 7). The negative sign can also be interpreted as a reduction in the faulted phase impedance shown in Fig. 9.

An important observation from this sequence network is that the negative-sequence network and the zero-sequence network are connected in parallel. This means that if a reactor has significant grounding impedance, I0 during a turn fault would be limited, whereas the I2 could be significant. These are typically reactors connected to the ungrounded transformer tertiary bus or four-reactor banks discussed in the introduction.

For low-grade turn faults, where the unbalance presented by the faulted reactor is small, the reactor presents a large impedance, and the system impedance is much smaller. This is evident from the real-world system parameters of Table I, where the system impedance is around 100 times smaller than the reactor impedance. However, in rare scenarios, it is also possible that for a line reactor during a contingency, such as a local line-terminal breaker open, the impedance of a long line presents a much larger zero-sequence impedance than negative-sequence impedance. While this larger system zero-sequence impedance is still much smaller than the reactor impedance, it reduces the system I0 for an internal fault compared to I2, lowering sensitivity for low-grade turn faults. This makes the use of I2 more favorable than I0 for turn fault detection.

Considering the larger zero-sequence impedances due to reactor grounding and those associated with transmission lines, it is preferable to use negative-sequence quantities for turn fault detection. The exception to this preference is inverter-based resource (IBR) applications, which are explained later in Section IV.F.

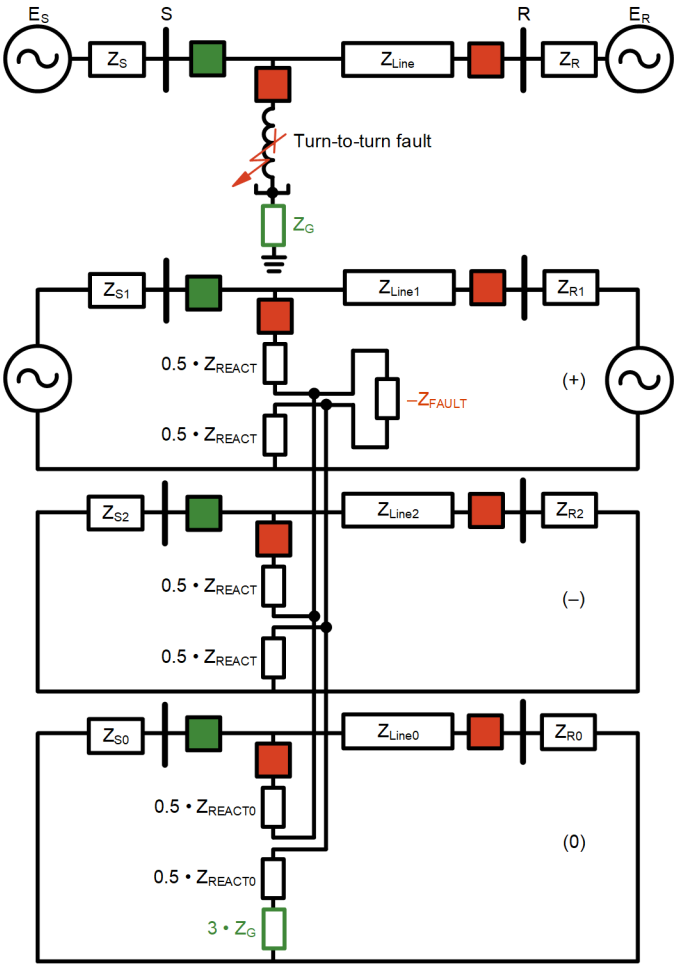

Fig. 11. Sequence network during a shunt reactor turn fault.

III. Overview of Reactor Protection Elements

This section briefly describes the protection functions covered in this paper. The functional overview is shown in Fig. 12. A combination of these functions can be used to provide comprehensive shunt reactor protection and is the focus of this paper. The neutral overcurrent elements (50/51N) and restricted earth fault (REF) element are not applicable to ungrounded or high-resistance grounded reactors. For these reactors, a zero-sequence overvoltage element (59G) is briefly discussed in this section but not shown in Fig. 12.

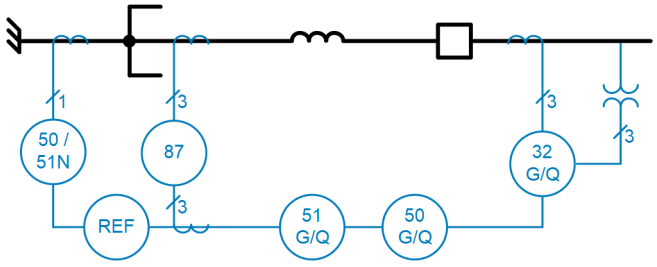

Fig. 12. Functional overview of shunt reactor elements.

Backup protection can be provided using nondirectional phase and sequence overcurrent elements, distance elements, and zero-sequence voltage differential elements [1] [2] [7] [14]. Because these elements provide reduced sensitivity and/or speed, they are not discussed in this paper. A high-impedance differential scheme [2] requires dedicated CTs and can provide primary phase and ground fault protection; it is not discussed in this paper.

A. Phase Fault Protection

The phase differential element for the purpose of this paper is illustrated in Fig. 13 [15] [16]. The element uses the terminal and neutral-side phase CTs to protect the reactor. The per-phase operate (IOPp) and restraint (IRTp) currents to the differential element are calculated by considering the terminal phase current (IpT) and neutral phase current (IpN), as shown in (2).

$$\begin{aligned} IOPp &= \left|IpT + IpN\right| \\ IRTp &= \left|IpT\right| + \left|IpN\right| \end{aligned} \tag{2}$$

For security, the element has an ac external fault detector (EFD) to detect a sudden and significant change in through current without an associated change in differential current (CONAC). The element also has a dc EFD that detects significant dc component in any of the zone currents (CONDC). On the rising edge of CONAC or CONDC, the differential gains security for 1 second. Additionally, a dc level in any of the signal continues to keep the differential in high-security mode.

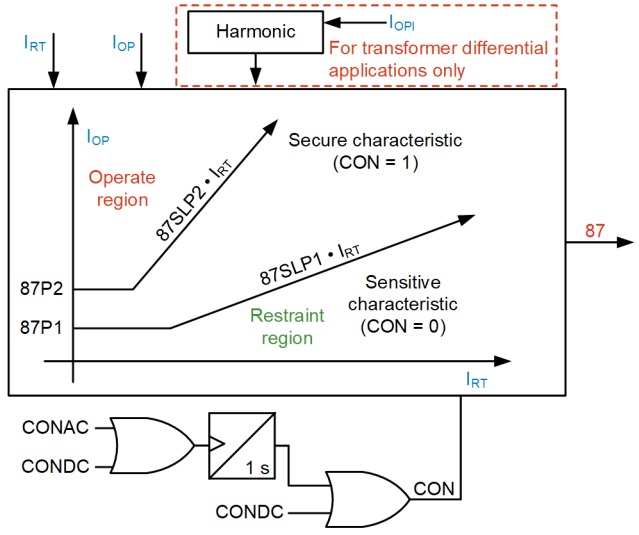

Fig. 13. Characteristic of a differential relay zone.

B. Ground Fault Protection

1) Solidly Grounded or Four-Reactor Banks

The differential element can also provide ground fault protection. To add sensitivity, the REF element is often applied and uses the terminal phase CTs and the neutral CT [17] [18]. The REF element logic is shown in Fig. 14, where REFF*n* is the forward internal fault trip indication. If there is sufficient 3I0 and IN, then RF*n*TCE asserts and the element can trip via the directional REF*n*FP path. If there is insufficient 3I0, the element can trip via the nondirectional NDREF*n* path.

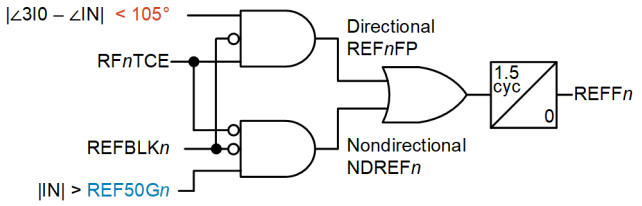

Fig. 14. REF element with directional and nondirectional paths [18].

For security, as shown Fig. 15, if there is a through or reverse 3I0 detected (REF*n*RP) or if there was a phase fault in the system (FLTP*n*) for an eighth cycle, then the element is blocked (REFBLK*n*) for 1 second [18].

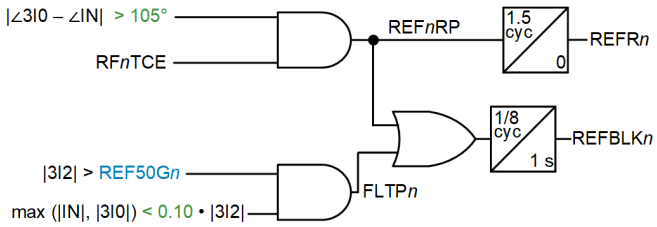

Fig. 15. Security measures for the REF element [18].

2) Ungrounded/High-Impedance-Grounded Banks

Ungrounded/high-impedance-grounded reactor banks are sometimes applied on the transformer tertiary bus. These reactors, often air-core, may have a grounding resistor on the secondary of a broken delta VT on the bus [14] [19] [20] (see Fig. 16).

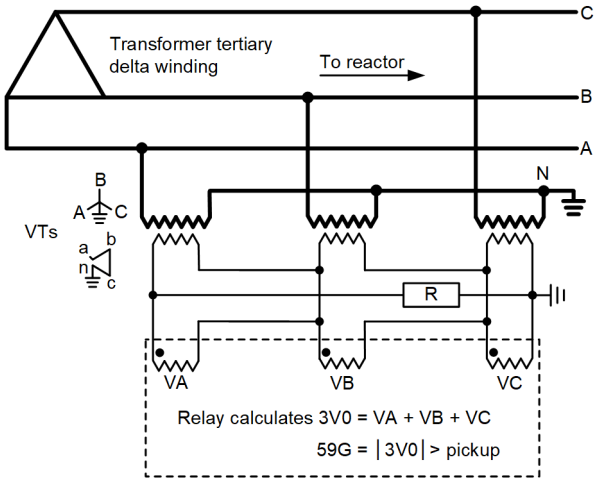

Fig. 16. Grounding resistor and bus ground fault protection [19].

The likelihood of ground faults in an air-core reactor is low. Therefore, a high-set zero-sequence overvoltage function (59G) is applied, typically to detect a ground fault on the bus, but it can also detect and alarm/trip for terminal-side ground faults on the reactor [2]. As explained in [19] via numerous field events, there is potential for severe damage, and the challenging response to "There is an alarm—what now?" that considers human safety, makes a strong case for tripping.

Ground faults in these ungrounded banks can be intermittent, and it is possible for ground faults to remain uncleared for a long duration without timing out [19]. The use of special timers, similar to those applied for stator ground fault

protection [21], can improve dependability by riding through dropouts associated with intermittent arcing behavior. The scheme is shown later in Section IV.D where the settings are discussed.

C. Turn Fault Protection

Turn fault protection has been proposed in the past using directional definite-time overcurrent elements [1] [22] [23]. The directional element logic using negative-sequence (Q) quantities is shown in Fig. 17. The three inputs to the two AND gates are described as follows:

- The top input checks that there is sufficient 3I2 compared to a forward or reverse pickup.
- The middle input verifies that the negative-sequence replica impedance (Z2 = V2/I2 shifted by the angle) is lesser or greater than the forward or reverse threshold.
- The bottom input checks that the ratio of the I2 relative to the positive-sequence current (I1) is greater than the natural unbalance of the reactor.

The 32Q element is supervised by a loss-of-potential condition, which is not shown in Fig. 17. The same logic applies to the zero-sequence directional element (32G).

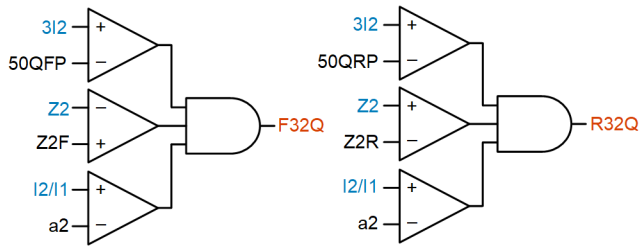

Fig. 17. Simplified negative-sequence directional element (32Q).

D. Protection Test Setup

For the simulations and playback of field events, we protect an EHV Reactor 1 and a MV Reactor 2. Reactor 1 is either solidly grounded or a four-reactor bank, depending on the illustration, whereas the MV reactor is ungrounded. For ease of testing, one relay protects both reactors with the terminal designations [16] [17] listed in Table IV. The voltages are measured at the bus, but they could be measured at the reactor terminals to achieve equivalent protection performance.

TABLE IV
CURRENT AND VOLTAGE TERMINALS

Terminal	Application	Usage
VpV	Reactor 1 terminal phase voltages	32Q
IpS	Reactor 1 terminal-side phase currents	87 Zone 1, REF, 67Q, 51Q
IpU	Reactor 1 neutral-side phase currents	87 Zone 1
IY3	Reactor 1 neutral current	REF
VpZ	Reactor 2 terminal phase voltages	32Q, 59G
IpT	Reactor 2 terminal-side phase currents	87 Zone 2, 67Q, 51Q
IpW	Reactor 2 neutral-side phase currents	87 Zone 2

IV. CT SIZING, SETTINGS, AND SECURITY

A. CT Requirements

1) General Considerations

Shunt reactors have unique CT requirements. Unlike with protection for equipment, such as generators, transformers, or buses, external faults are not a concern for shunt reactor protection because the associated fault current levels are low. On the other hand, reactor banks are often switched frequently, on a daily basis in many systems. Shunt reactor energization currents, unless using point-on-wave (POW) closing, can be characterized by their large and long-lasting dc offsets from high X/R ratios. Due to the frequency of the switching, the possibility of a large remanence left in the CT and the likelihood of encountering an unfavorable energization instant that challenges protection are greater.

Normally, CT saturation in shunt reactor applications is thought to have a security and sensitivity impact on the differential element, but the differential element is inherently very sensitive (see Section V.A), and the impact of CT saturation is relatively low when the differential is set with a bias toward security (see Section IV.B). However, CT saturation has a great impact on turn fault protection due to the high sensitivity requirements (see Section II.C). This paper provides simple guidelines for using system parameters to develop settings, similar to the approach first presented in [15] for generator applications.

2) CT Dimensioning—Ratio and Voltage Ratings

To maximize turn fault protection sensitivity, it is preferable to select a low CTR so that the reactor rated current is close to the relay current input ratings [22]. Heavy internal faults are not a concern because, even if the CT saturates or if the fault currents are beyond the relay's data acquisition range, protection can operate quickly to isolate the fault.

On the other hand, tapping down a multiratio CT can reduce the effective accuracy class, which can then increase measurement errors during reactor inrush due to dc CT saturation. A simulated air-core reactor inrush is shown in Fig. 18.

The remanence in the CTs prior to the energization is unbalanced [24] so that the C-phase saturates first, the A-phase saturates next, and the B-phase saturates last. This type of remanence may be expected if the reactor is energized at a similar point-on-wave twice. The steady-state reactor currents post energization do not eliminate remanence but can reduce it to a certain extent when operating near the knee point [15] [25].

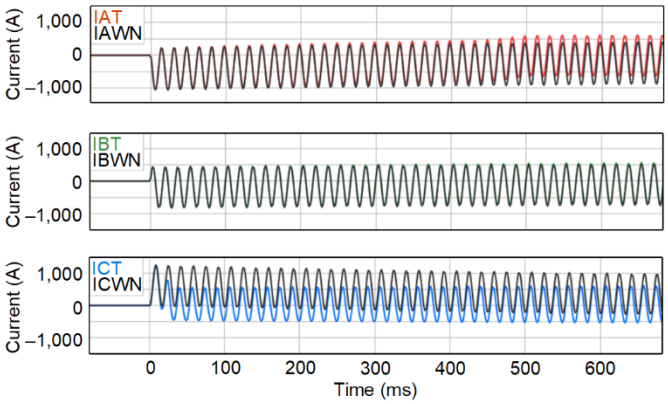

Fig. 18. Simulated air-core reactor inrush with heavy dc CT saturation.

The magnitude ratio and angle errors for the C-phase current of Fig. 18 are shown in Fig. 19. The magnitude error is ~20% and the phase error is ~35°. The CT saturation in the different phases also results in a 3I2 of ~60%. The neutral current does not have any measurement error because the primary system is balanced.

An exponential characteristic with the reactor X/R ratio is overlaid on the magnitude plot. We see that the error is not related to the X/R ratio of the reactor—the error decays quicker initially, but slower after 4 seconds. This is because the CT saturation error is related to the CT time constant, which is short when the CT is in its saturated region but long in the linear region. The time constant of closed-core CT is in the order of 10 seconds [15]; therefore, a 30-second delay is adequate for the error to become negligible.

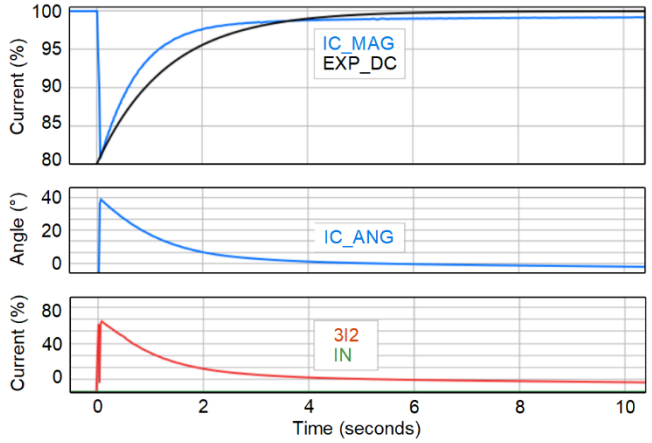

Fig. 19. Phasor measurement errors due to CT saturation during inrush.

The worst-case magnitude ratio and angular error with CT remanence up to 95% are shown in Fig. 20. The errors are represented as a function of an inrush dimensioning factor (K_{INRUSH}) calculated using (3), where V_{SAT} is the saturation voltage, R_{CT} is the CT resistance, and R_B is the burden [15].

$$K_{INRUSH} = \frac{V_{SAT}}{(I_{RATED} / CTR) \cdot (R_{CT} + R_B)} \quad (3)$$

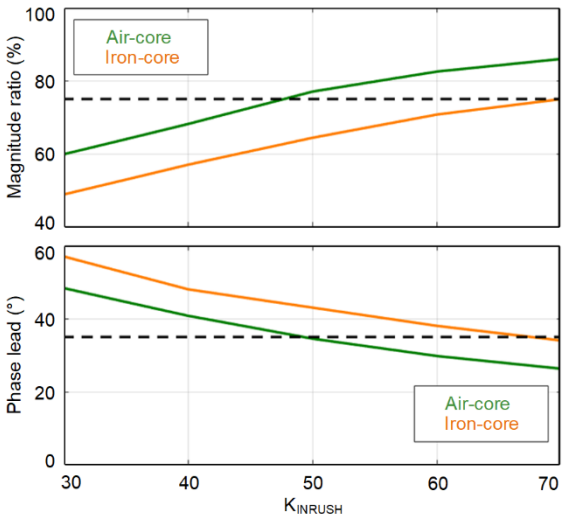

Fig. 20. Worst-case magnitude ratio (top) and phase lead (bottom) as a function of K_{INRUSH}.

Most CTs in the field are applied with a K_{INRUSH} greater than the values shown in Fig. 20. For example, a C400 200:5 CT with an RCT of 0.1 ohm has a minimum V_{SAT} of 404 V [15]. Assuming an I_{RATED} of 200 A and R_B of 0.5 ohm, we calculate a K_{INRUSH} of 135. To be conservative, we limit the upper range to 70 because a relay's internal CT can also saturate due to the decaying dc [15]. The associated magnitude ratio is 75% (i.e., 25% error) with a phase lead of 35° (see dashed black lines in Fig. 20). If CTs are tapped down or sized such that their associated K_{INRUSH} could result in greater magnitude and phase errors, then larger errors should be considered when developing protection settings.

Overall, the general recommendation for CT sizing is to minimize the CTR such that relay settings accommodate the desired sensitivity, but not reduce the CTR so much that K_{INRUSH} evaluates to a value less than 70, which would then require desensitizing settings for adequate security.

Based on the setting guidance later in Section IV.C and Section IV.E, sensitive reactor protection settings use values of 6% of the reactor rating, whereas the setting ranges in relays may be limited to a value of 5% to account for steady-state errors. Therefore, we recommend using a CTR such that the reactor rated current (I_{RATED}) in secondary amperes is greater than 83.5% (5% divided by 6%) of the relay nominal current. If it is difficult to achieve a K_{INRUSH} greater than 70 due to a low CTR, one option is to select a relay with a lower current input rating (e.g., 1 A current terminals in a 5 A application) [26].

B. Percentage-Restrained Reactor Phase Differential (87)

1) Myths and Misunderstandings

Reactor switching may be performed daily in some systems, and it is important to have security during reactor inrush. The most common misunderstanding is that harmonic restraint or blocking functions, as used by a transformer differential element, secure a reactor differential element, due to harmonics in the currents that are present during iron-core reactor energization but not during air-core reactor energization [4] [27]. The harmonic security features in a transformer differential element act on the differential current associated with the transformer inrush; this is described in Fig. 21a, where only CT1 sees the inrush current. However, for a reactor energization (see Fig. 21b), the current passes through both CTs and the differential current is zero. Therefore, no security is gained, irrespective of the reactor type. Any security from harmonic restraint or blocking methods occurs after CT saturation from the long-lasting dc offset during energization. However, there is no guarantee that there will be significant harmonics in the currents. This is shown in Fig. 22 using a field event record of an iron-core reactor inrush [27] with negligible second and fourth harmonics throughout the event despite a differential current appearing after 1.5 seconds.

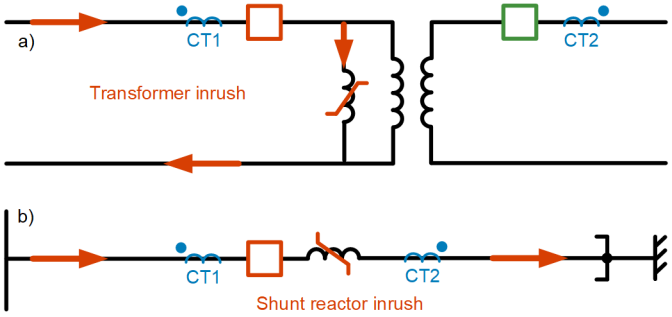

Fig. 21. Inrush current passing through a) one CT for transformer differential and b) both CTs for reactor differential.

Another misunderstanding is the reliance on the ac EFD, described in Section III.A, for all forms of CT saturation. The ac EFD is not ideal for security due to CT saturation during shunt reactor inrush, which can last several seconds, as evident from the field event of Fig. 22 [27]. The ac EFD in the differential expires after 1 second, whereas the slow dc CT saturation occurs after 1.5 seconds, when ac EFD has expired. The ac EFD is an incremental technique that looks for a sudden change in currents, and the dropout timer may not be long enough for systems with high X/R ratios.

The dc EFD adds security in Fig. 22 for as long as the dc in the differential zone currents is high. However, after the dc disappears between 1.5 and 1.8 seconds in Fig. 22, because of dc CT saturation, a differential current appears. This same loss of dc causes the dc EFD to expire, as is evident from the CONBDC1 and CONB1 deassertion. An additional dropout timer to extend security from the dc EFD is helpful if the differential element is set very sensitively and users rely on the dc EFD to provide security.

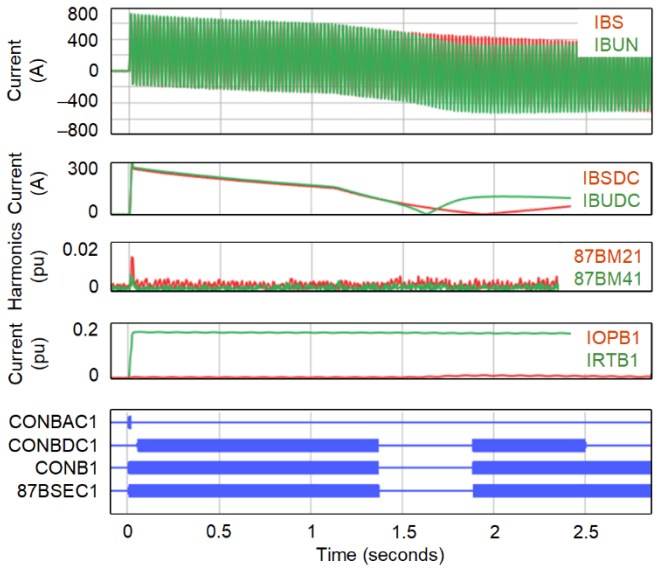

Fig. 22. Relay playback of a field iron-core reactor energization.

A final issue is reduced dependability when relying on the EFD to supervise sequence-quantity-based turn fault protection [2] [7]. While the EFD is phase-segregated, it can assert on the A-phase if the A-phase currents change sufficiently because of a fault on the B-phase or the C-phase [28]. For a turn fault, it can even assert on the faulted phase, because, without CT saturation, there is no differential current due to a turn fault. This can block protection for heavy internal turn faults [29]. The EFDs are tailored to the differential element, and it is important to be careful when using them for other applications, such as sequence-quantity-based protection.

2) Settings Guidelines

The settings guidelines depend on the relay design. When using a relay with ac and dc EFDs and using delays to extend security, the Slope 1 setting may be set to ~10% to account for steady-state errors, and the Slope 2 setting may be set to 35% or higher for adequate security, considering the 25% magnitude error and 35° phase lead, as calculated in (4).

$$\text{Slope with CT saturation} = \frac{\text{IOP}}{\text{IRT}} = \frac{\left|1 - 0.75\angle 35°\right|}{1 + 0.75} \sim 33\% \qquad (4)$$

Many relays do not have these external fault detectors, and more importantly, as will be shown in Sections V.A and V.B, a slope setting does not limit sensitivity for phase fault protection or even ground fault protection in solidly grounded systems. Therefore, for simplicity, a Slope 1 setting of 35% and a Slope 2 setting of 50% are secure for CT saturation, are dependable for internal faults, and are recommended and used in this paper.

The percentage slopes depend on the definition of the restraint current [30]. For instance, if the restraint current is half the sum of the zone current magnitudes, Slopes 1 and 2 would be 70% and 100%, respectively. If the restraint is the maximum of the zone currents, then Slopes 1 and 2 could be 60% and 80%, respectively.

C. Restricted Earth Fault (REF)

The REF element should be set above the maximum expected unbalance [18]. As noted in Section II.B.1, reactor unbalance can result in a maximum 3I0 of 3.46% for a solidly grounded reactor bank. By adding a margin, we calculate a value of 6% of the reactor rating. This value can then be converted to the REF element pickup setting (REF50G), as shown in (5).

$$\text{REF50G} = 0.06 \text{ pu} \bullet \frac{I_{RATED}}{\left(\text{CTRN} \bullet I_{NOM\_CTRN}\right)} \quad (5)$$

Four-reactor banks have a neutral reactor that limits 3I0. Therefore, they can be set even more sensitively (6).

$$\text{REF50G} = 0.06 \text{ pu} \bullet \frac{I_{RATED}}{\left(\text{CTRN} \bullet I_{NOM\_CTRN}\right)} \bullet \left(\frac{X_1}{X_1 + 3X_N}\right) \quad (6)$$

The above values are limited by a minimum relay setting of 0.05 pu to account for steady-state errors.

D. Zero-Sequence Overvoltage (59G)

The zero-sequence overvoltage scheme with the sequencing timer discussed in Section III.B.2 is shown in Fig. 23. The pickup level has a typical value of 70% of the voltage for a phase-to-ground fault on the bus [20].

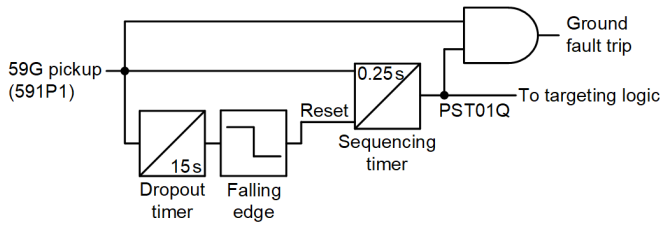

Fig. 23. Sequencing timer used to improve dependability for intermittent faults.

The scheme of Fig. 23 uses a sequencing timer [16] [17] to ride through intermittent ground faults, although other timers available to digital relays can also be used [21]. The sequencing timer pickup delay may be set to a value ranging from 0.25 seconds [19] up to 80% of the thermal capacity of the grounding resistor [20]. The reset time of the sequencing timer may be set to 15 seconds. The timer accumulates toward the trip time of 0.25 seconds when 59G picks up. If the input does not assert for 15 seconds, then the timer resets with aid from the dropout timer. The use of the sequencing timer is more important when the element is set with a long pickup time delay.

E. Directional Overcurrent Scheme

The turn fault protection scheme designed for optimum security, sensitivity, and speed using functions available in most digital relays is shown in Fig. 24. The basic principle is that the overcurrent element is set to remain secure for CT saturation, whereas the directional element provides security for external events. Additional security to the scheme is provided by the logic of Fig. 25.

The associated application-dependent settings guidelines are shown in Table V and are based on the following principles:

- A neutral CT is a valuable addition for reactor turn fault protection, as noted in [31]. The measured neutral current (IN) is inherently secure for any CT saturation, and when available, its use allows protection to be set with minimal time delays.
- There is no primary system I0 or I2 associated with air-core reactor inrush, as explained in Section II.B.2. Therefore, the protection can be set with short time delays.

The operating principle of the Fig. 24 scheme is:

- Zone 1 provides fast protection and is enabled at all times. The pickup is set above the worst-case CT saturation, reactor inrush, and reactor unbalance.
- Zone 2 is sensitively set with an IN or 3I2 value of 6% (I0 or I2 of 2%), which provides a 73% security margin over the maximum possible reactor unbalance of 1.15%. Security is primarily achieved from the arming delay, which enables this zone 10 to 30 seconds after the reactor is energized, or if there is an external event.
- The 51 element is slow but active at all times, just like Zone 1, and remains dependable when Zone 2 is disarmed. The pickup and time dial are set to coordinate with the worst-case errors associated with CT saturation and reactor inrush.

All three levels are supervised by the logic of Fig. 25, with the principles explained as follows:

- A three-phase overcurrent supervision ensures that the scheme can only trip when the reactor bank is online (PSV24) [1]. A pickup of 75% of I_{RATED} has adequate dependability margin for system undervoltage conditions. A three-phase overcurrent is preferred to an undervoltage supervision [2], because it remains dependable for high-magnitude turn faults, as shown in Section V.C.1 through the use of a field event. Additionally, an undervoltage supervision requires VTs at the reactor terminals, which are not always available. This supervision also adds security for a breaker open pole due to pole-scatter during energization or because a pole is stuck. It uses the same currents required for a 3I2 calculation to confirm measurement validity, including a CT failure.
- The protection only responds to reactor internal/forward faults (F32Q), which ensures security for any external events.
- The sensitive Zone 2 is only armed during a steady-state condition. For solidly grounded iron-core reactors, this is associated with the primary system X/R ratio of approximately 2 seconds, for an overall arming delay of 10 seconds. For ungrounded reactor banks where 3I2 is used, the errors can last longer and are associated with the time constants of CTs, which can be around 10 seconds for closed-core CTs [15]. Therefore, a 30-second arming delay is used.

For all the settings guidelines provided in this section, it is preferable to confirm during commissioning that the composite asymmetry of the reactor and from the CTs is sufficiently less than the pickup settings during steady state (i.e., more than 30 seconds after reactor energization). The approach used by Avista to verify the standing asymmetry and deploy these settings to their air-core reactor is shared in Section IV.J, with the settings detailed in Appendix B. Based on our analysis, extensive simulator testing, and field experience, the settings of Table V are secure. However, if additional security is desired, the various pickups and time delays can certainly be increased. If increasing security, it is beneficial to consider the protection speed preference of oil-immersed iron-core reactors. A more thorough evaluation using the approach of Section V.C.5 can help with the tuning process and development of optimized settings.

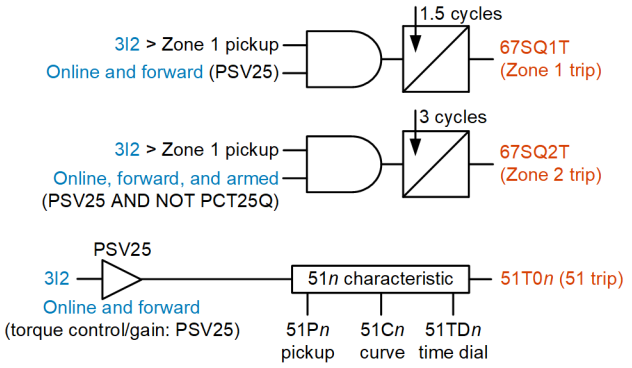

Fig. 24. Turn fault protection scheme.

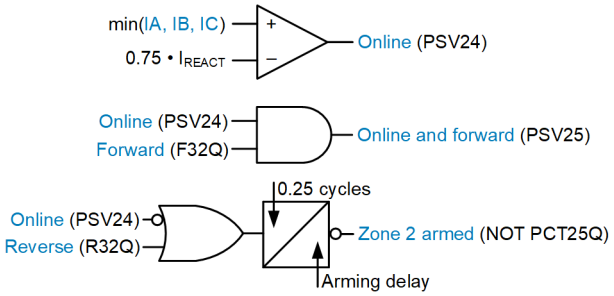

Fig. 25. Auxiliary logic to add security to turn fault protection scheme.

TABLE V
DEFAULT SECURE AND SENSITIVE OVERCURRENT SETTINGS FOR SHUNT REACTOR TURN FAULT PROTECTION (FOR USE WITH FIG. 25)

Reactor Type*	50/51 Current Used	50/67 Zone 1	50/67 Zone 2	51 Inverse-Time
Solidly grounded air-core	Neutral current (IN)	Pickup: 6% Delay: 1.5 cycles	NA	NA
Solidly grounded iron-core	Neutral current (IN)	Pickup: 50% Delay: 1.5 cycles	Pickup: 6% Delay: 3 cycles Arming delay: 10 seconds	Pickup: 6% Curve: U2 Time dial: 2.5
Ungrounded air-core	Negative-sequence current (3I2)	Pickup: 80% Delay: 1.5 cycles	Pickup: 6% Delay: 3 cycles Arming delay: 30 seconds	Pickup: 10% Curve: U2 Time dial: 6
Ungrounded iron-core	Negative-sequence current (3I2)	Pickup: 170% Delay: 1.5 cycles	Pickup: 6% Delay: 3 cycles Arming delay: 30 seconds	Pickup: 10% Curve: U2 Time dial: 7

Note—Four-reactor bank protection scheme can gain dependability by using both IN and 3I2 (see Section V.C.4).

1) *Directional Element Settings*

The 32Q element of Fig. 17 provides security for external system unbalances and is set such that:

- The forward and reverse overcurrent pickup settings, 50QFP and 50QRP, are equal to 6% of the rated reactor current to match the minimum settings from Table V.
- The a2 setting (I2/I1) is set to 2%, which provides a margin above the maximum unbalance of 1.15%. It is important to note that a2 uses I2, whereas the overcurrent elements use 3I2 and are set at the minimum at 6%, three times this 2%. A small a2 setting has been suggested in the past to provide dependable turn fault protection in shunt reactors [32] and generator stators [29].
- The Z2F setting is set to 50% of the reactor impedance (Z_{REACT}) and the Z2R is set just above it [22].

2) Overcurrent Element Settings

The overcurrent element settings in Table V are obtained assuming worst-case CT saturation, including burden and remanence, unfavorable reactor bank asymmetry of ±2%, and point-on-wave of breaker closure. The expected operating times are shown as a function of operate current in Fig. 26 for a 60 Hz system. For solidly grounded air-core reactors, the operate time is 1.5 cycles for a current greater than 6%. For the other reactors, when the current is greater than 6% and when Zone 2 is armed, the operate time is 3 cycles.

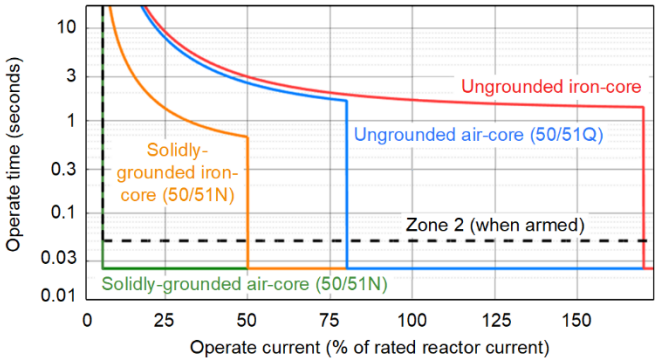

Fig. 26. Expected protection operate times for different reactors.

The Zone 1 pickup levels of Table V are evaluated based on the dashed trace of Fig. 20. With the 75% magnitude ratio and 35° phase error, we calculate a maximum possible 3I2 of 80%. This occurs when:

IA = 1 pu ∠0°

IB = 0.75 pu ∠–120° + 35°

IC = 1 pu ∠120° + 35°

If K_{INRUSH} is lower than 70, then the associated adjustment based on Fig. 20 can be performed.

The 51 characteristic choice is based on several thousands of simulated test cases with hardware-in-the-loop that checks the maximum time dial required for security. The 51N element operating on IN can ride-through iron-core reactor inrush with a relatively low pickup of 6% and a short time dial of 2.5. The 51Q element operates on 3I2, has to also remain secure for CT saturation, and requires a higher pickup of 10%. Secure settings for the 51Q element for a simulated iron-core reactor inrush are shown in Fig. 27. The inverse-time 51Q curves integrate the higher inrush levels initially and, therefore, need to be set more securely than the alternative definite-time 50Q levels. However, we prefer the simplicity afforded by a single 51Q curve to add dependability at different fault levels. The IEEE U2 curve is used because it is secure at high current levels, for which Zone 1 is relied on. This curve's moderately inverse shape allows faster operation than some of the other curves.

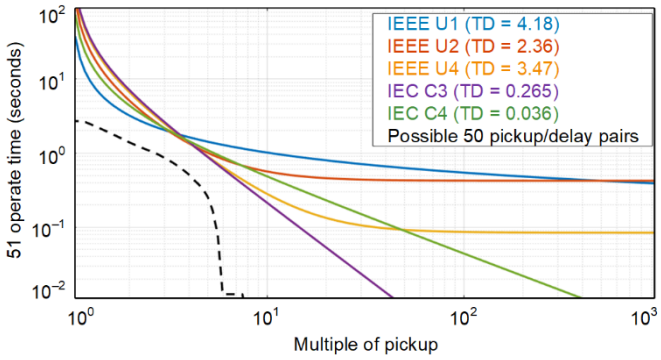

Fig. 27. Secure 50 and 51 characteristics for an iron-core reactor inrush.

The 51Q U2-curve time dials that provide secure operation for a K_{INRUSH} of 30 to 70 with 10° increments are 9, 7, 5, 3.5, and 2.5, respectively. As stated previously, the guidance is based on an a K_{INRUSH} of 70 with a secure time dial of 2.5. In Table V, we add considerable margin to get the time dial of 6 and 7 for an air-core and iron-core reactor, respectively. If K_{INRUSH} is lower than 50 to 70, for instance, then the time dial should be increased.

F. Application Considerations for Directional Overcurrent Scheme

1) Line Reactors

When a transmission line is de-energized, there is a ringdown phenomenon in which the distributed capacitance of the line exchanges energy with the line reactors [1] [33] [34]. With the power system disconnected, the natural ringdown frequency (f_{LC}) of this oscillation can be approximated by (7) using the shunt capacitive reactance (X_C) and the shunt inductive reactance (X_L) of the line evaluated at the system frequency (f_{SYS}). For example, if a line reactor is sized to compensate 75% of the capacitive reactance at an f_{SYS} of 60 Hz, then f_{LC} evaluates to 52 Hz, per (8).

$$f_{LC} = f_{SYS}\sqrt{\frac{X_C}{X_L}} = f_{SYS}\sqrt{\frac{MVAR_L}{MVAR_C}} \quad (7)$$

$$f_{LC} = 60\ \text{Hz} \bullet \sqrt{0.75} = 52\ \text{Hz} \quad (8)$$

When the line is de-energized after a fault, the voltage on the faulted phases are depressed and the associated reactor phase currents may be lower than the 75% current threshold of Fig. 25 (see Section IV.H.2). However, when the line is normally de-energized (without a fault), the phase voltages and currents may increase and there is a step-change in frequency from f_{SYS} to f_{LC} (see Section IV.H.1). Normally, power system frequencies ramp because of system inertia, according to the swing equation. Relays are often designed to assume this power system characteristic of frequency ramps [16] [17]. The frequency step-change during line reactor de-energization can result in phasor estimation errors and cause a misoperation of the turn fault protection scheme of Fig. 24.

To provide security during ringdown (following normal line de-energization), one option is the use of line breaker statuses to block protection [1]. If only the local line terminal breaker status is used, then the scheme can lose dependability when the line is energized from the remote terminal, similar to the scenario of Fig. 11. If the remote line terminal breaker status is also used, then the scheme has communications channel requirements [1]. The protection scheme can be degraded, due to a loss of the channel, consideration of channel latency, and possible reduced reliability of breaker statuses.

A simple solution to secure the scheme of Fig. 24 for line reactors is to use the frequency tracking capabilities of modern relays [16] [17] to detect frequency deviations. When a sudden frequency change occurs, the healthy frequency indication (FREQOK) in the relay deasserts quickly, well before the shortest pickup time delay of 1.5 cycles. After the frequency measurement (FREQ) is restored and FREQOK asserts, the relay accurately tracks f_{LC}. These signals can be used for the frequency supervision (FREQSUP) logic of Fig. 28 and can be used for additional supervision of the ONLINE logic of Fig. 24 If other relays are used that have different signals available to provide frequency supervision, then the pickup time delay of the turn fault protection scheme requires coordination with the frequency supervision.

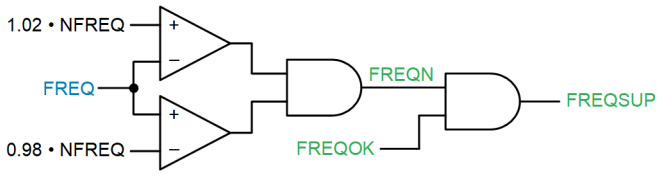

Fig. 28. Frequency supervision for line reactor turn fault protection.

The FREQSUP logic provides security during unreliable frequency measurement, when FREQOK is deasserted. The frequency is usually calculated from the measured voltages. If the VTs measure voltages at the reactor terminals, the FREQSUP logic using FREQOK can take around a few cycles to assert, which can delay a Zone 1 turn fault protection trip during a reactor switch-on-to-fault scenario. Therefore, it is preferable to use the line VTs (on the line-side of the reactor breaker).

The FREQSUP logic also secures the protection scheme of Fig. 24 when f_{LC} is outside 2% of f_{SYS}. In applications where the reactor is sized to compensate within 95% to 105% of the capacitive reactance, f_{LC} may be within 2% of f_{SYS}. In such cases, the ringdown during line de-energization is fairly smooth and the turn fault protection scheme of Fig. 24 is inherently secure. Therefore, the FREQSUP logic of Fig. 28 can be generally used to supervise turn fault protection for line reactors, and the logic provides security during ringdown as needed.

2) Reactor Bank Grounding

The use of the 32Q element for directionality is preferred to the use of zero-sequence directional element (32G), because it is independent of the reactor grounding. Additionally, the negative-sequence impedance of the grid is also usually lower, allowing for better protection performance during contingencies in a weak grid, as explained in Section II.D.

3) High Penetration of IBRs and IBRs in Weak Grids

For shunt reactors in an IBR plant bus with a very weak grid, the use of the 32Q element can reduce protection element performance. For the scheme of Fig. 24, the concern is primarily related to dependability. For an internal fault, the I2 phase angle could vary and make an internal fault look as if it were external [35]. The IBR could also inject very little I2. Even for standardized IBRs that are required to inject I2 during unbalanced faults, the system voltage change may not be significant enough during low-grade turn faults for the IBR to start injecting any I2. On the other hand, bus-connected shunt reactors in an IBR plant often have a strong zero-sequence path presented by a nearby grounding bank. Therefore, for solidly grounded shunt reactors in an IBR plant, the use of the 32G element is preferable to the 32Q element. For shunt reactors connected to the ungrounded IBR plant transformer tertiary bus, the zero-sequence voltage differential scheme may be used [1] [7] [14]; although, it may provide reduced sensitivity and/or speed compared to the directional overcurrent scheme discussed in Section IV.E.

4) Variable Shunt Reactors (VSRs)

VSRs are becoming popular in some systems due to maintenance, space, and economic considerations [8]. These reactors are equipped with an on-load tap changer and a regulating winding that allow them to provide variable reactive power compensation, for instance, from 50% to 100% of their maximum rating. The guidance provided in this section is based on 100% of the maximum rating, which can limit dependability when the reactor is tapped down to a lower value. In these applications, the online check of Fig. 25 should have the current threshold reduced to 75% of the minimum VSR rating. In addition, a 1-cycle delay should be added to Zone 1 and Zone 2 of Fig. 24 to compensate for the reduced security. If the fast 1.5-cycle and 3-cycle time delays for Zone 1 and Zone 2 are to be retained (for instance, to mitigate a fire hazard in an iron-core reactor) then additional zones with different overcurrent supervision levels and delays may be added, or an input from the tap-changer controls can be used, to make the scheme adaptive.

5) Unbalanced Power Systems

In rare applications, the power system can be unbalanced such that V2 and I2 are greater than 2%. In such applications, the scheme of Fig. 24 can still be applied. However, Zone 2 can remain blocked and provide reduced dependability due to the unbalanced V2 and I2 asserting R32Q consistently. In such cases, Zone 2 may be supplemented, or replaced, by a normalized negative-sequence operating quantity, V2/V1 minus I2/I1, as first presented in [36] and later applied in [7]. In addition to the scheme design considerations presented in [7], we recommend the additional security from Fig. 25, with the exception of the R32Q input. We think such unbalanced systems are rare, and supplementing Zone 2 with the normalized negative-sequence method should be based on

profiling the power system using field measurements, similar to the approach presented in Section IV.J.

G. Identifying the Faulted Phase for Targeting

The reactor current is inductive and the fault current that is partly dependent on the system impedance is usually also inductive. Therefore, the faulted phase current magnitude increases during a fault, which then increases the sequence components.

The behavior of the phasors for an A-phase turn fault in a solidly grounded reactor is shown in Fig. 29, with the I1, I0, and I2 during the fault near 0°. For a B-phase fault, I1 is about 0°, I0 is about –120°, and I2 is about +120°. The angle difference between sequence currents can then be compared to determine the faulted phase. Relays often use I0 and I2 to identify the faulted phase [17], but the presence of I0 may be misinterpreted for ground fault involvement. This can be resolved by verifying an operation of the REF element.

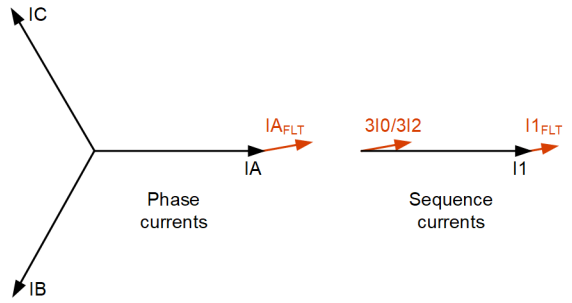

Fig. 29. Phase and sequence current phasors for an A-phase fault.

For four-reactor banks, I0 is reduced and may not be sufficient to help faulted phase identification. In ungrounded reactor banks, the faulted phase current splits to the unfaulted phases, whereas I0 is negligible and unusable. Therefore, for simplicity and generality, it is preferable to compare I2 and I1 for faulted phase identification. The exception is in solidly grounded reactors in IBR plants with possibly unreliable I2, where the preference is to compare I0 with I1.

In ungrounded reactors, it is possible for the 59G element to trip for either a ground or turn fault. However, there is no I2 for a ground fault in ungrounded reactors. Therefore, a 59G trip without an associated 67Q trip can be used as an indication of ground involvement.

For the field installation discussed in Section IV.J, the generic scheme comparing I2 and I1 was used, with the implementation details shared in Appendix B. For the purpose of this paper, this is the version used for fault-type identification.

H. Line Reactor Protection Security During Line De-Energization and Ringdown

1) Security During Normal Line De-Energization

A normal line de-energization is simulated and shown in Fig. 30, where the last line breaker is opened at t = 0. Because the three-poles of the breaker do not open at the same time and because of the difference between f_{LC} and f_{SYS}, there is an unbalance in the circuit that develops and appears in the neutral of the shunt reactor. The relay continues to incorrectly track the system frequency of 60 Hz for some time, and this results in erroneous phasor estimation, as evident from the high magnitude ripple in the 3V2 and 3I2. Even though the unbalanced 3V2 (at a frequency of f_{LC}) is in the reverse direction, the relay declares forward because of the phasor estimation error. FREQOK drops out a quarter cycle after the relay declares a forward fault, so using FREQSUP that considers FREQOK ensures that the turn fault protection of Fig. 24 scheme remains secure.

At ~80 ms, FREQOK asserts, the relay tracks the frequency to f_{LC} of ~52 Hz, and FREQN deasserts to provide security. After the filter transients, the phasors stabilize and the directional element starts to see the unbalance in the reverse direction correctly. During the ringdown, FREQSUP remains deasserted, either due to a deassertion of FREQOK or FREQN, and adds security to line reactor turn fault protection.

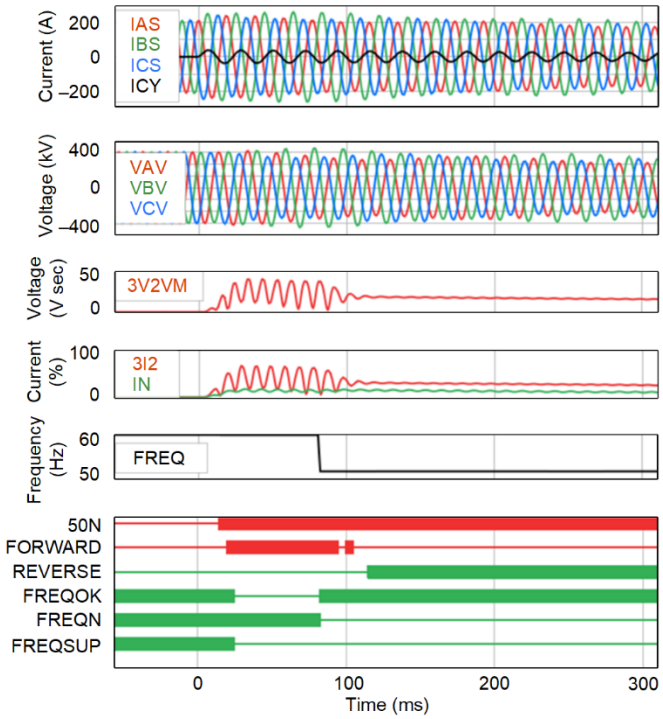

Fig. 30. Security provided by frequency-based supervision during line de-energization and ringdown.

2) Security During External Faults and Reclosing

The behavior of many of the other security mechanisms is summarized and illustrated using the simulation of Fig. 31 for a solidly grounded air-core line reactor.

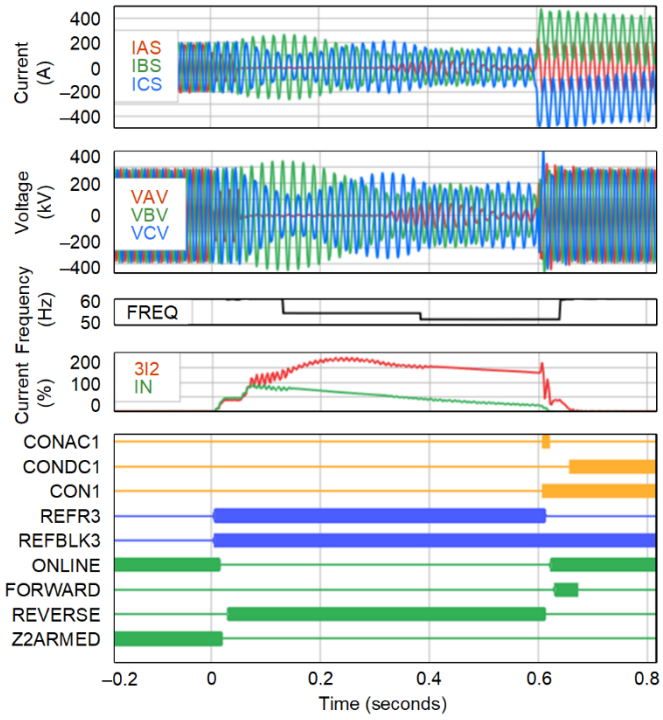

Fig. 31. Security features during an external fault and reclosing event.

A line AG fault occurs on the line at t = 0. The A-phase voltage sags due to the fault causing an associated reduction in the reactor A-phase current. The online indication requires all three-phase currents, so it deasserts shortly after, which, in turn, disarms Zone 2. The reverse indication from the 32Q element also asserts for the reverse fault, as does the reverse indication from the REF element (REFR3). An REFR3 assertion causes an assertion of the REFBLK3 bit, which secures the REF element. The EFD does not assert because there is not a sufficient change in current to require security for CT saturation.

Once the line breakers trip at ~50 ms, ringdown voltages and currents appear on the unfaulted phases. The A-phase voltage and current remain at zero because the fault still exists until ~0.3 seconds. The ringdown voltages and currents associated with the resonance of the line capacitance and the shunt reactors are at an off-nominal frequency, going down from the nominal 60 Hz to a value of ~52 Hz.

A high-speed reclose is initiated at ~0.6 seconds. The online indication asserts shortly after all three currents are healthy and present. The forward indication from the 32Q element asserts for 40 milliseconds during energization. The neutral current, however, is already zero by the time forward asserts. The 3I2 during this time is lower than 42%, which is well below a 3I2 of 80% for a negative-sequence Zone 1 if applied. Zone 2 pickup is 6%, but it is disarmed for another 30 seconds. None of the turn fault protection elements get an opportunity to time on their 1.5- or 3-cycle timers. The REF element is blocked for another 1 second since REFR3 has recently asserted. The reactor inrush currents have very high dc offset in the B- and C-phases, resulting in a loss of zero-crossings for the remainder of the event. This high dc current can cause dc saturation of the terminal- and neutral-side phase CTs eventually, while the neutral CT remains unsaturated. The ac EFD initially asserts due to the sudden surge in currents, and the dc EFD asserts shortly after to prevent a misoperation due to dc saturation.

I. Iron-Core Reactor Misoperation Postmortem Analysis for Italian Transmission System Operator—Terna S.p.A.

A field event of a challenging iron-core reactor inrush that resulted in a misoperation of the differential is shown in Fig. 32 [27]. Due to dc CT saturation, there is magnitude attenuation of ~22% and a phase lead of ~27° that remains until there is a misoperation and the reactor bank trips. The operate current increases to a slope of ~25.5%. The 3I2 value reaches a value of 48.5%.

This is the most severe field event of dc CT saturation we have seen. A slope of 35% for the differential element and a 3I2 pickup of 170% for our Zone 1 turn fault protection, consistent with our settings guidelines, ensure adequate security from the protection elements.

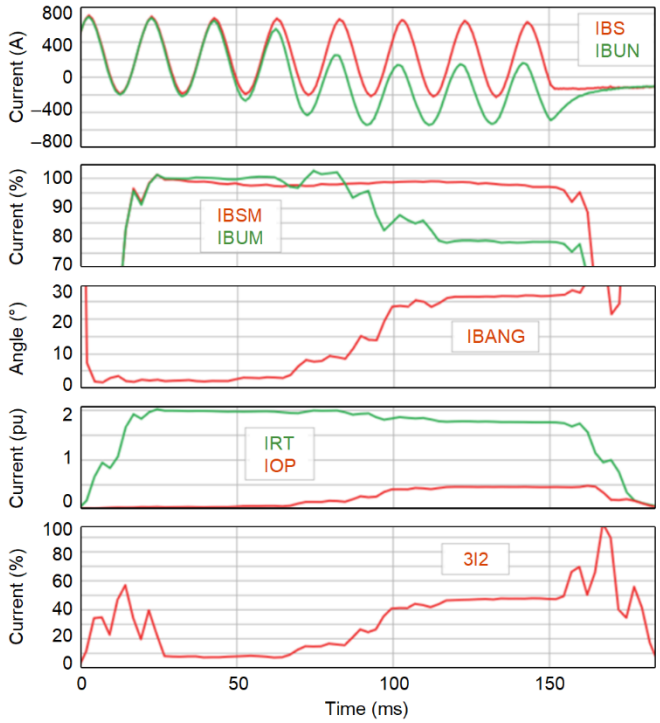

Fig. 32. Challenging field event of an iron-core reactor inrush.

J. Avista Field Experience With Air-Core Reactor Protection

Avista has solidly grounded bus-connected air-core reactors, which allowed for testing most of the guidelines provided in this paper. We configured the settings in monitoring mode for several weeks. In monitoring mode, we recorded the profile of several signals, which provided a snapshot of the system every 5 minutes. The profile of several signals during a day is shown in Fig. 33. The reactor is online from 2:20 a.m. to 7:25 a.m. For reference, the unbalance for a reactor could be up to an I2 of

1.15% from Section II.B.1, and our sensitive settings are based on an I2 of 2% from Section IV.E.

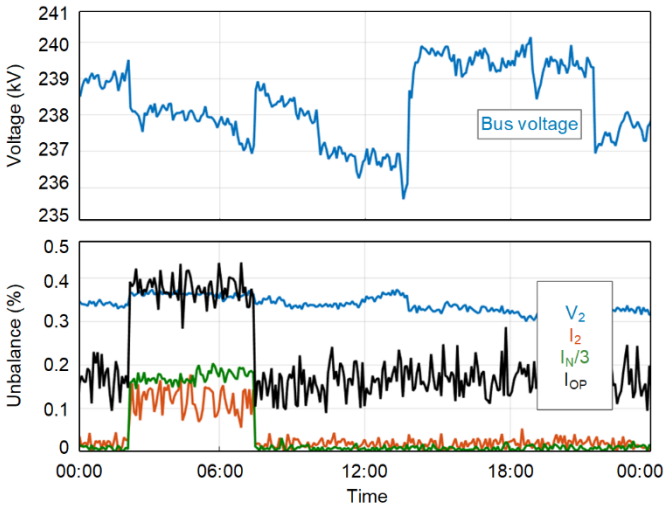

Fig. 33. Measured profile of several signals throughout one summer day.

From the profile, we can see that the I0 measured at the neutral (IN/3) is less than 0.2%. The neutral current is indicative of a primary system unbalance, either from the reactor or the system voltages. This unbalance of 0.2% is well below the maximum reactor unbalance of 1.15% and our setting thresholds of 2%. The I2 is nearly equal to I0; therefore, the measurement error on the phase CTs is negligible.

The V2 is at a higher value of 0.35%, which might be a combination of the system unbalance and measurement errors. If this value were greater than 2%, we might have considered supplementing our turn fault protection Zone 2 with a method that can compensate for the unbalance [7] (see Section IV.F.5).

The differential element operate current, shown as a maximum of the per-phase values, reaches a value of 0.4% or 0.004 pu. This is well below the applied pickup of 0.30 pu.

After the monitoring period, we set the relay to trip the breaker with the settings presented in Appendix B. Not shown in the Appendix, but we also configured additional monitoring settings that provide higher sensitivity and speed to alarm for a possible near miss. An AG field event with the protection settings deployed to trip is shown in Fig. 34.

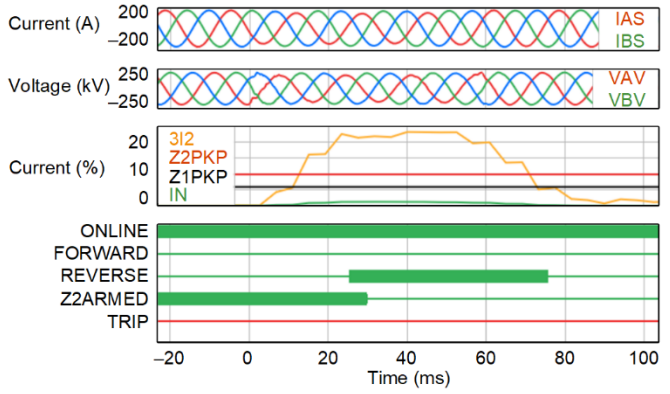

Fig. 34. Reverse field AG fault from field with reactor online and settings deployed.

Our experience from the many switching and fault records has been great. We have not come close to a near miss, which, along with our extensive testing, gives us full confidence in the security of our protection schemes and settings guidelines.

V. Dependability Evaluation

This section demonstrates the dependability, including sensitivity and speed, for internal faults as provided by the different protection elements discussed in this paper. Field events of air-core reactor turn faults received from Xcel Energy [7] and RTDS simulations using the new model described in Section II.C [10] are used to illustrate protection performance.

A. Phase Faults

A phase-to-phase fault that is 1% from the neutral on the B-phase and 1% from the neutral on the C-phase is simulated in the EHV iron-core reactor (see Fig. 35). The differential (87R1) trips in 12 ms. The terminal phase currents see a visible increase in fault currents, which translates to a 3I2 of 375%. The neutral phase currents increase to almost 100 times the value. The presence of the neutral phase CTs makes the differential extremely sensitive. The targeting logic identifies a BC phase fault accurately.

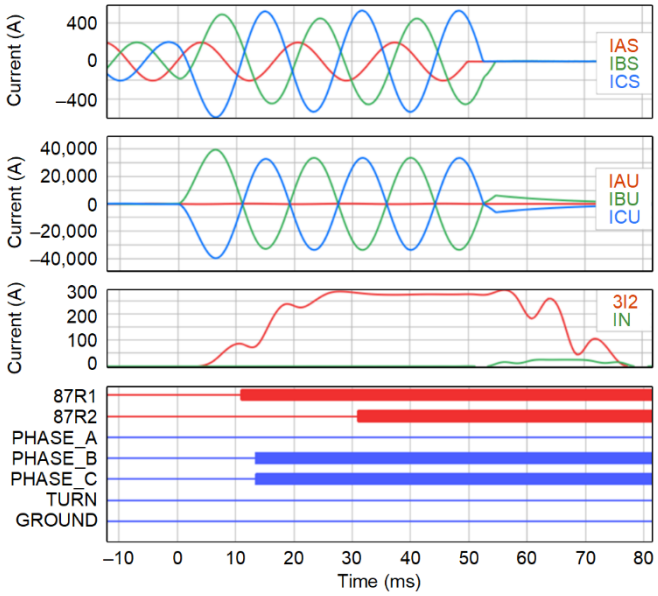

Fig. 35. Phase fault near the neutral (1% to 1%) of an iron-core reactor.

For comparison, we enable the Zone 2 differential with the same pickup and slope but also enable harmonic blocking and restraint functions with default second and fourth harmonic percentages (15%) associated with a transformer differential. We can see that Zone 2 trips in 31 milliseconds, compared to the Zone 1 trip of 11 milliseconds. Zone 2 is slow to trip because the step change in fault current has to propagate through the harmonic filters [37]. Possible CT saturation, not shown in the figure, could further slow down a harmonic-based differential element. A delayed trip presents fire hazards to an iron-core reactor. As explained in Section IV.B, it is much better to use conservative slope settings for security rather than relying on harmonic functions that are not likely to help. To

emphasize the point, the slope in Fig. 35 was practically 100% because the neutral phase current dominated the response of the differential element.

A phase fault in an air-core reactor is unlikely and not shown in the figure. The general behavior is the same as in Fig. 35, although the fault currents are much lower. For instance, the neutral phase current still dominates the response of the differential element but has about a tenth of the fault current level as the iron-core reactor.

B. Ground Faults

1) Solidly Grounded Reactor

The protection response for an AG fault 1% from the neutral of an air-core reactor is shown in Fig. 36. Similar to the phase fault of Fig. 35, there is a lot of neutral-side phase current, and the differential element operates quickly. There is also a lot of neutral current, which allows the turn fault protection to trip on Zone 1. However, there is not a lot of change in terminal-side currents, resulting in a small 3I2 and 3I0; they are about one-hundredth of IN. The REF element is set sensitively and operates on the directional path by comparing the angle of 3I0 and IN. If 3I0 is insufficient, for instance, for a fault at a lower percentage of the winding or for a resistive fault, then the REF element could operate on the nondirectional path based on the IN magnitude (see Fig. 14). Generally speaking, the REF element does not add significant protection sensitivity to the differential element in solidly grounded reactor banks, similar to its application in power transformers [18]. It does, however, help the targeting logic identify a ground fault accurately.

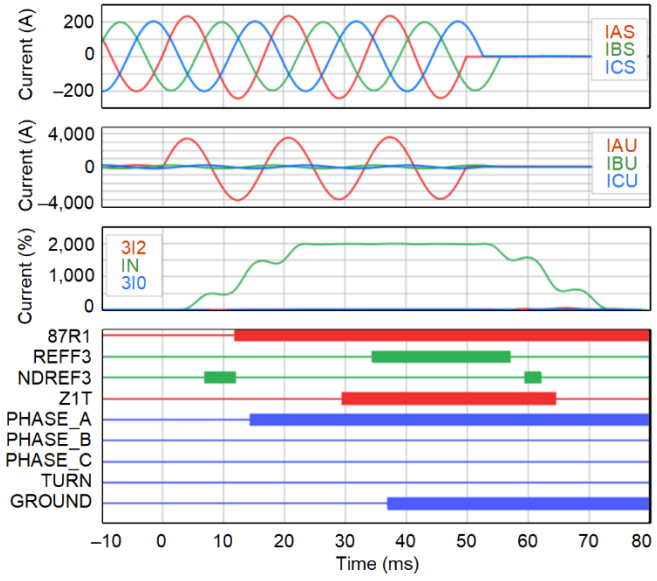

Fig. 36. Ground fault near the neutral (1%) of an air-core reactor.

2) Four-Reactor Bank

Placing an AG fault 1% from the neutral results in no trip. The protection response for an AG fault 2% from the neutral of a four-reactor air-core bank is shown in Fig. 37. The terminal A-phase current very slightly increases in magnitude, whereas the neutral A-phase current slightly decreases. Therefore, considering the CT polarities, the associated 3I0 and IN are in phase with one another, and the REF element marginally operates.

The turn fault protection does not measure sufficient 3I2 to operate for this fault. The differential element sees an operate current of 0.12 pu and a restraint current of 2 pu, resulting in a slope of 6%, which is significantly lower than the 35% required to trip. A lack of operation from the differential for the fault of Fig. 37 results in suboptimal targeting showing that a ground fault occurred, but not which phase was involved.

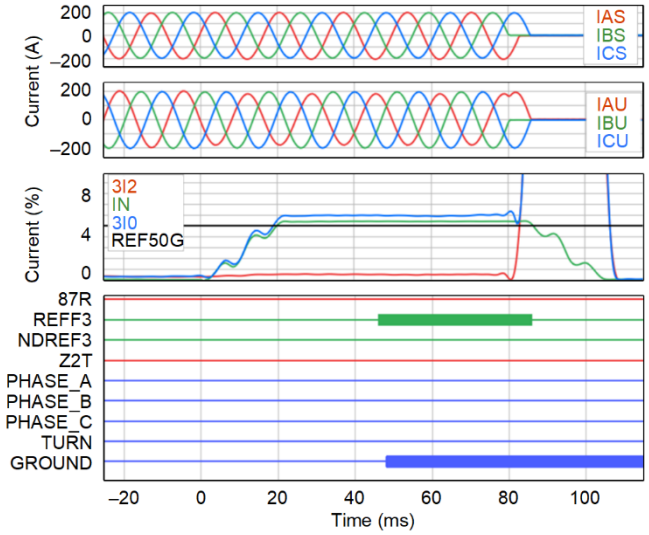

Fig. 37. Ground fault near the neutral (2%) of a four-reactor bank.

Eventually, both the differential and turn fault protection operate when the fault is placed 10% from the neutral (not illustrated in this paper). The differential element operate current is 0.67 pu, and the restraint current is 1.66 pu for a fault that is 10% from the neutral. The targeting logic works optimally once the differential element starts to operate.

The sensitivity provided by the REF element is more helpful for four-reactor banks than for solidly grounded reactors, but the REF element's sensitivity gain relative to the differential element is not as significant as it is in low-impedance grounded transformers and generators [18].

3) Ungrounded Reactor

An intermittent AG fault at the terminal of a 13.8 kV reactor is shown in Fig. 38. The arcing fault logic from [29] is used for the simulation. Every time the fault arc is established, the zero-sequence volage is equal to the negative of the faulted phase voltage. The pickup is set to 70%, and the element picks up and drops out throughout the event. The output of the element using a normal pickup timer (591P1T) does not trip, but the output of the sequential timer (PST01Q) trips.

The targeting logic behaves correctly. While not detailed in the paper, it is similar to the targeting logic of Section IV.G. The difference is that we compare the angle between the zero-sequence and positive-sequence voltage, and the voltage angles are the opposite of turn fault current angles because the voltage drops, unlike the turn fault currents that rise.

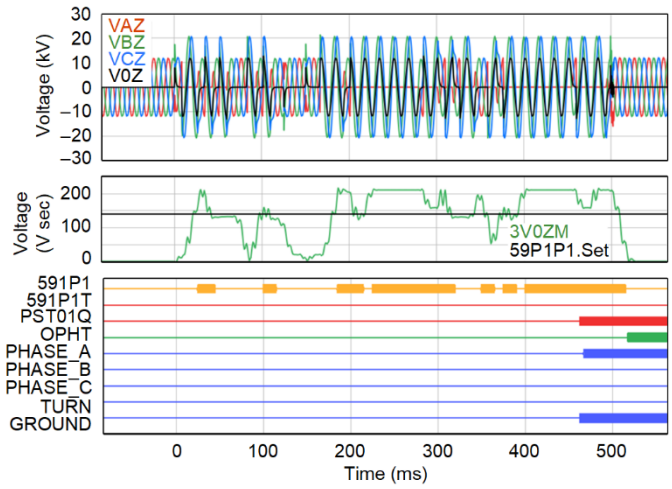

Fig. 38. Intermittent ground fault at ungrounded reactor terminal.

C. Turn Faults

1) Ungrounded Air-Core Reactor

On November 12, 2017, a turn fault occurred on an ungrounded 50 MVAR air-core reactor connected to the delta tertiary of a 448 MVA, 345/115/34.5 kV autotransformer at Xcel Energy [7]. We received and replayed the event record through the relay [17] (see Fig. 39). The Zone 2 arming logic delay of Fig. 25 was removed to better illustrate Zone 2 performance, knowing that the reactor was online prior to the event.

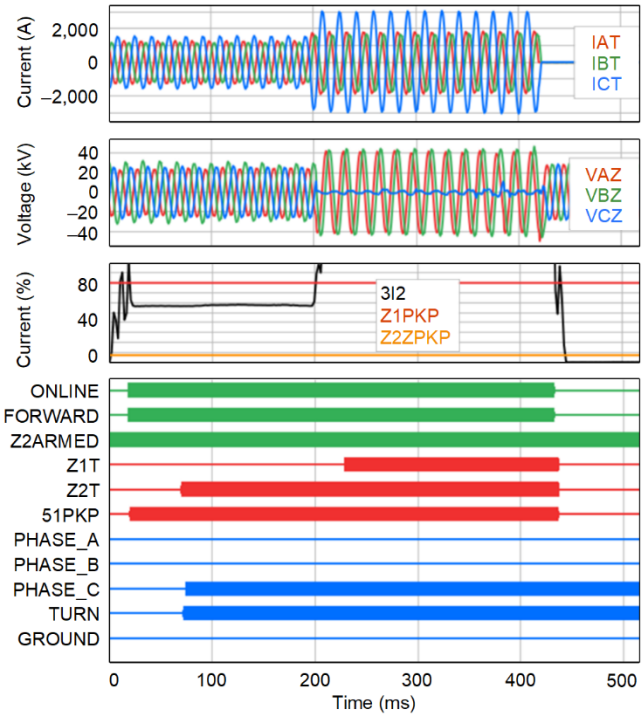

Fig. 39. Relay playback of a field turn fault on an ungrounded reactor.

The turn fault was already present when the event started recording. The 3I2 value in the measured data is 57%, which is much higher than the Zone 2 and 51 pickup levels but lower than the Zone 1 pickup of 80%. Zone 2 trips in 3 cycles after the online and forward indications assert. The targeting logic indicates a C-phase turn fault. After the fault evolves such that the 3I2 level becomes 237%, Zone 1 trips in 1.5 cycles.

2) Solidly Grounded Air-Core Reactor

On April 14, 2018, a turn fault occurred on a solidly grounded 25 MVAR air-core reactor connected to a 115 kV bus at Xcel Energy [7]. We received and replayed the event record through the relay [17] (see Fig. 40). Based on the setting guidance from Table V, only Zone 1 with a low pickup of 6% is applied. The neutral current (IN) hovers around 40% initially, allowing Zone 1 to trip 1.5 cycles after the filter transient. The targeting logic indicates an A-phase turn fault accurately. As expected from a solidly grounded reactor, both 3I2 and IN are equal. This fault evolves gradually, unlike the sudden evolution in the event of Fig. 39.

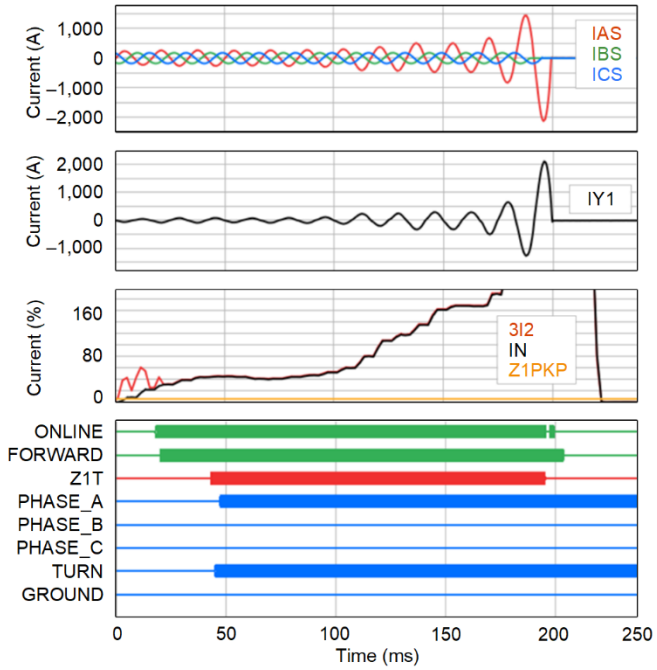

Fig. 40. Relay playback of a field turn fault on a solidly grounded reactor.

A simulated turn fault that shorts 1% of the A-phase turns of a solidly grounded air-core reactor is shown in Fig. 41. The neutral current is less than 20%, which is still higher than the Zone 1 pickup of 6%, and the reactor trips quickly. The targeting logic indicates an A-phase turn fault accurately.

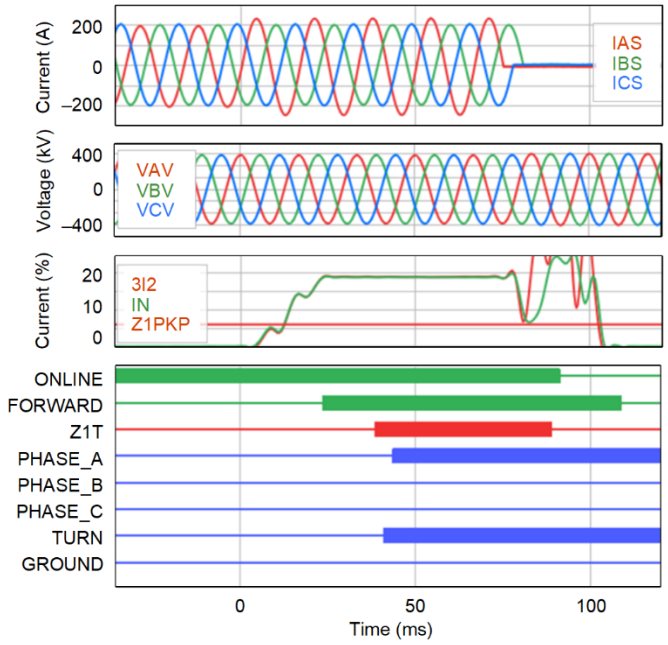

Fig. 41. Turn fault (1%) on a solidly grounded air-core reactor.

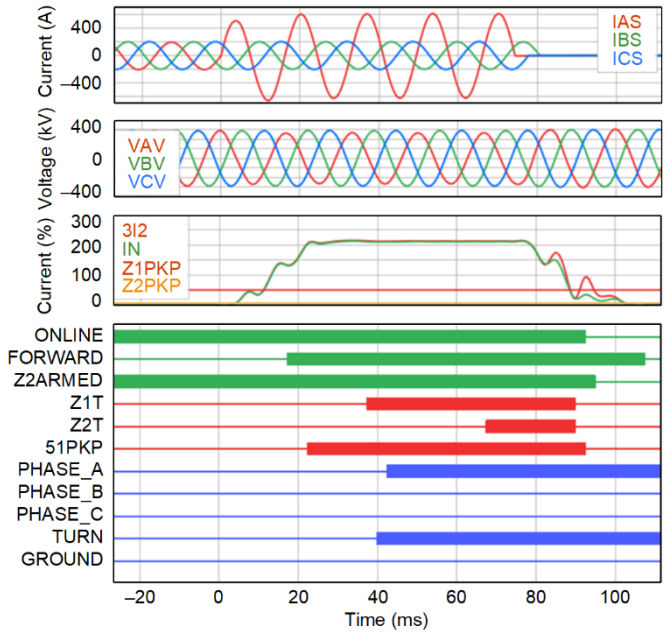

Fig. 42. Turn fault (1%) on a solidly grounded iron-core reactor.

3) Solidly Grounded Iron-Core Reactor

A simulated turn fault that shorts 1% of the A-phase turns of a solidly grounded iron-core reactor is shown in Fig. 42. As with the solidly grounded air-core reactor, the turn fault protection elements use the neutral current to operate (see Table V). The IN during the fault is ~210%, which allows Zone 1 set at 50% to trip after a 1.5-cycle time delay. The targeting logic indicates an A-phase turn fault accurately.

The measurable currents during an iron-core reactor turn fault is significantly higher than the measurable currents in the equivalent air-core reactor turn fault shown in Fig. 41. This allows protection to provide higher sensitivity for iron-core reactor turn faults, as discussed in Section V.C.5.

4) Four-Reactor Iron-Core Bank

The same fault of Fig. 42 is simulated in a four-reactor bank and is shown in Fig. 43. For the turn fault protection, both IN and 3I2 are used based on Table V. The neutral reactance allows the neutral-point voltage to shift, which reduces the measurable currents during a turn fault. Compared to Fig. 42 with IN and 3I2 of ~210%, IN now reduces to ~76%, whereas 3I2 reduces to ~159%. If Zone 1 were using only 3I2, it would not have tripped due to a high pickup of 170%, whereas a Zone 1 using IN trips due to a lower setting of 50%. Using IN improves protection speed in this scenario. However, the behavior could be different in another reactor bank, because the magnitude of 3I2 versus IN are dependent on the ratio of the neutral-to-phase reactance of the four-reactor bank.

If a smaller percentage of turns were shorted, then it could be possible for IN during the fault to be less than the Zone 2 pickup, whereas 3I2 could be higher. In such scenarios, using both IN and 3I2 can result in increased protection sensitivity.

These considerations demonstrate the dependability gains of using both IN and 3I2 as the operating signal when protecting four-reactor banks.

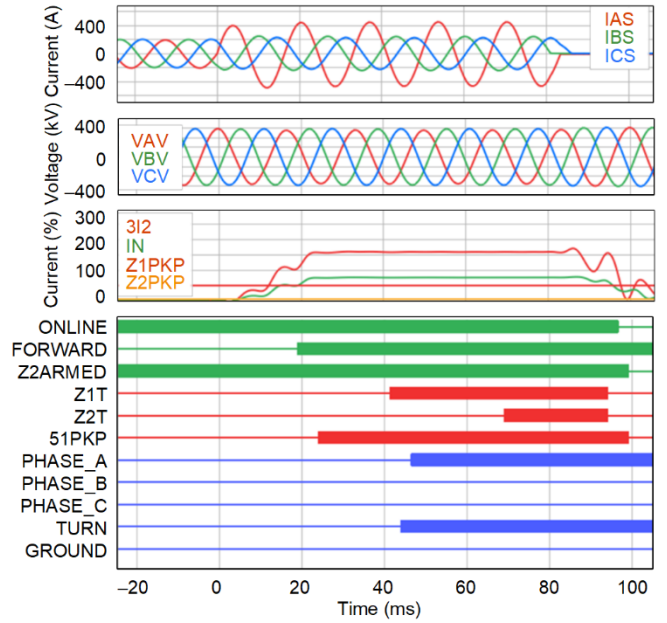

Fig. 43. Turn fault (1%) on a four-reactor iron-core bank.

5) Turn Fault Protection Sensitivity Summary

The performance of the different protection elements of Table V are summarized in Table VI. The reactor types are obtained from Table II and Table III. An MV iron-core reactor is not shown because we did not have the data (as they are seldom used for modern MV tertiary-bank applications).

The sensitivity estimates are from Fig. 8, based on the model of Appendix A, and are approximate in nature. They are intended to offer a sense of the coverage provided by the protection elements and are summarized as follows.

- For the ungrounded MV air-core reactors (1A and 2A), the Zone 2 and 51 elements can detect a single turn fault. Zone 1 only detects the fault once it has evolved significantly to 15% of the phase. The vast difference between the sensitivity provided by Zone 1 and Zone 2 emphasizes the extremely nonlinear fault response and the benefit of using a faulted reactor model (see Appendix A) to estimate coverage.
- For the solidly grounded EHV air-core reactor, we can detect a fault that shorts 8 turns when using older designs (3B), whereas we can detect fewer turns with modern designs (3A).
- For the solidly grounded iron-core reactor (3I), the Zone 2 and 51 elements can detect down to 2 turns, whereas Zone 1 can detect down to 6 turns.

As noted in Section IV.E, the approach shown here using the reactor-type, grounding, and reactor parameters may be used to tune the setting guidelines from Table V. However, the model of Appendix A is simplified and only offers an estimate. Furthermore, it is also possible for the reactor unbalance noted in Section II.B.1 to decrease during a turn fault. For instance, if the A-phase has the highest inductance of 1.02 pu, then an A-phase turn fault could make the reactor bank more balanced. This unbalance can be profiled to some degree using the method of Section IV.J. Considering the various sources of inaccuracies, it is, therefore, suggested to use adequate margins if tuning the protection settings.

TABLE VI
SENSITIVITY OF TURN FAULT PROTECTION SCHEME OF TABLE V

Reactor Type	Grounding Method	50/67 Zone 1	50/67 Zone 2	51 Inverse-Time
1A (air-core 13.8 kV)	Ungrounded	15% (14 turns)	0.19% (1 turn)	0.28% (1 turn)
2A (air-core 34.5 kV)	Ungrounded	15% (32 turns)	0.19% (1 turn)	0.28% (1 turn)
3B (air-core 238 kV)	Solidly grounded	0.2% (8 turns)	NA	NA
3A (air-core 238 kV)	Solidly grounded	0.2% (5 turns)	NA	NA
3I (iron-core, 230 kV)	Solidly grounded	0.3% (6 turns)	0.1% (2 turns)	0.1% (2 turns)

VI. CONCLUSION

Sensitively set shunt reactor protection schemes are required to remain secure for reactor inrush and external system events.

Turn faults are a common fault type, especially in air-core reactors. Security is challenged due to saturation of an iron-core reactor and CT saturation in all reactors and is discussed in Sections II.B and IV. Sensitivity for an air-core reactor can be challenged due to the behavior of magnetic flux, number of turns, and physical layout, and is discussed in Section II.C. Speed is more important for iron-core reactors due to possible fire hazards. The scheme of Fig. 24 uses a directional overcurrent Zone 1, Zone 2, and an inverse-time characteristic, which allows maximizing sensitivity and speed while maintaining security. The settings guidance for this scheme is provided in Table V. Several application considerations, such as line reactor ringdown, grounding, IBRs, VSRs, and unbalanced power systems are discussed in the associated Section IV.F. Security for line reactor ringdown is provided using a novel method that uses local relay measurements. The current pickup for these values corresponds to a 3I2 or IN value of 6% (I2 of 2%), which allows them to detect faults that short around 0.1% of turns in an iron-core reactor and 0.2% of turns in an air-core reactor. The analysis that helps determine the fault currents and approximate sensitivities is discussed in Section II.C and Section V.C. Simplified MATLAB and Mathcad tools are provided in Appendix A to help estimate approximate fault currents.

Phase faults are sensitively detected by the differential element (see Section V.A). A differential element set securely, such as with a slope setting of 35%, can detect faults down to 1% of the winding due to the high phase currents measured by the neutral-side CTs. If additional sensitivity is desired, a dc level detector with a long dropout delay may be added for security. In such cases, the slope settings can be reduced down to lower values, such as 10%.

Ground faults in solidly grounded reactor banks are sensitively detected by the differential element. For four-banks used in transmission line single-phase tripping applications, an REF element adds sensitivity for ground faults near the neutral. For ungrounded reactors, the use of timers available in digital relays can add dependability for intermittent ground faults. These are illustrated in Section V.B.

The protection methods are demonstrated to provide adequate security (see Section IV), using simulations and field events. These settings have also been deployed in Avista with great field experience; the settings are shared in Appendix B. Dependability for internal faults is shown in Section V using RTDS simulations on a new shunt reactor model and field events of turn faults. Faulted phase identification for targeting is shown to be simple and accurate.

VII. ACKNOWLEDGEMENTS

We thank Pratap Mysore, Adi Mulawarman, and AJ Donati from Xcel Energy for sharing the field events of air-core reactor turn faults used in this paper. We thank Charles Henville for his careful review and helpful comments. We also thank Andrea Di Tomasso for sharing field events and data from an iron-core reactor deployed by the Italian transmission system operator.

VIII. Appendix A: Electromagnetic Circuit Equations for Air-Core and Iron-Core Reactor Turn Faults

A simplified faulted circuit is represented by Fig. 44.

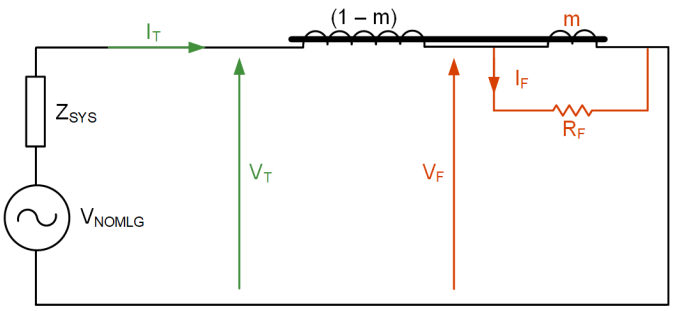

Fig. 44. Equivalent circuit used for analysis of turn fault.

The faulted voltage (V_F) can be represented by the fault path, determined by (9). The key equations (9), (15), (21), and (22) are distinguished in red font and are used in the matrix of Fig. 45 and the MATLAB and Mathcad programs of Section VIII.A and Section VIII.B.

$$0 = V_F - R_F I_F \tag{9}$$

V_F is also equal to the voltage induced by the flux per (10), where m is the per-unit turns shorted in the reactor and R_L is the resistance of the reactor.

$$V_F = m\left[N\left(\frac{d\phi}{dt}\right) + R_L\left(I_T - I_F\right)\right] \tag{10}$$

The flux in (10) is the sum of the flux due to the current from the faulted turns and the mutually coupled term from healthy turns (M_{TF}), as represented by (11). Taking the derivative and extracting the angular frequency term, as shown in (12), we can substitute the physical parameters with the reactor impedance, per (13). By collecting the terms of (13), we calculate (14).

$$N\left(\frac{d\phi}{dt}\right) = \mu N^2\left(\frac{A}{l}\right)\left(m\frac{d\left(I_T - I_F\right)}{dt} + (1-m)M_{TF}\frac{dI_T}{dt}\right) \tag{11}$$

$$N\left(\frac{d\phi}{dt}\right) = \mu N^2\left(\frac{A}{l}\right)j\omega\left[m\left(I_T - I_F\right) + (1-m)M_{TF}I_T\right] \tag{12}$$

$$N\left(\frac{d\phi}{dt}\right) = X_L\left[m\left(I_T - I_F\right) + (1-m)M_{TF}I_T\right] \tag{13}$$

$$N\left(\frac{d\phi}{dt}\right) = \left[m + (1-m)M_{TF}\right]X_L I_T - mX_L I_F \tag{14}$$

By substituting (14) to (10) and collecting the terms to help represent in matrix form, we calculate (15).

$$0 = -V_F + m\left\{\left[\left(m + (1-m)M_{TF}\right)X_L + R_L\right]I_T - \left[mX_L + R_L\right]I_F\right\} \tag{15}$$

The healthy branch voltage can be represented per (16).

$$V_T - V_F = (1-m)\left[N\left(\frac{d\phi}{dt}\right) + R_L I_T\right] \tag{16}$$

We repeat the same approach as (11) through (14) for the healthy winding, as shown in (17) through (20).

$$N\left(\frac{d\phi}{dt}\right) = \mu N^2\left(\frac{A}{l}\right)\left[(1-m)\frac{dI_T}{dt} + mM_{FT}\frac{d\left(I_T - I_F\right)}{dt}\right] \tag{17}$$

$$N\left(\frac{d\phi}{dt}\right) = \mu N^2\left(\frac{A}{l}\right)j\omega\left[(1-m)I_T + mM_{FT}\left(I_T - I_F\right)\right] \tag{18}$$

$$N\left(\frac{d\phi}{dt}\right) = X_L\left[(1-m)I_T + mM_{FT}\left(I_T - I_F\right)\right] \tag{19}$$

$$N\left(\frac{d\phi}{dt}\right) = \left[(1-m) + mM_{FT}\right]X_L I_T - \left(mM_{FT}X_L\right)I_F \tag{20}$$

By substituting (20) to (16) and collecting the terms to help represent in matrix form, we calculate (21).

$$0 = V_F - V_T + (1-m)\left\{\left[\left(1 - m + mM_{FT}\right)X_L + R_L\right]I_T - \left[mM_{FT}X_L\right]I_F\right\} \tag{21}$$

The power system impedance (Z_{SYS}) affects VT, and it can be represented by (22). Z_{SYS} can be determined by applying a phase-to-ground fault at the reactor terminals in a short-circuit program. For air-core reactors, the coupling with the other layers and the impedance associated with coils in the unfaulted stacks can be considered with additional equations, but is not included in this paper for simplicity. Reactor bank grounding can also be added in a similar manner.

$$V_{LN} = V_T + Z_{SYS}I_T \tag{22}$$

The mutual inductance terms, M_{TF} and M_{FT}, are lower for an air-core reactor than an iron-core reactor. They are calculated per (23) and (24) based on the height and the radius of the faulted coil and any other mutually coupled coils. The method assumes that the flux from the extremities of the healthy or faulted subwinding bends circularly with the radius of the coil once it leaves the cross-section (see Fig. 7). Using the radius is conservative and assumes that the fault occurs either at the neutral or the terminal; terminal-side turn faults are most likely because of possible reignition transients [38]. If the fault occurs in the middle of the coil, then the mutual inductances in (23) and (24) can be calculated by replacing the radius with the diameter, and the fault currents increase accordingly. The assumption is similar to the approach presented in [39] and as used by Carter to calculate slot leakage in electric machines [40].

$$M_{TF} = \left(\frac{\text{Radius}}{\text{Height}}\right)\bullet m + (1-m)\bullet M_{MAX} \tag{23}$$

$$M_{FT} = \left(\frac{\text{Radius}}{\text{Height}}\right)\bullet(1-m) + m\bullet M_{MAX} \tag{24}$$

The overall matrix has the form of (25).

$$\begin{bmatrix}0\\0\\0\\V_{LN}\end{bmatrix} = \begin{bmatrix}\text{Equation 9}\\\text{Equation 15}\\\text{Equation 21}\\\text{Equation 22}\end{bmatrix}\begin{bmatrix}V_F\\I_F\\I_T\\V_T\end{bmatrix} \tag{25}$$

A. MATLAB Program for Faulted Reactor Model

The MATLAB program for the faulted air-core reactor model with the parameters in Table I and assuming a single stack is provided as follows. Executing the program results in the output shown in Table VII.

The "Rtype" variable should be changed to "Iron" for an iron-core reactor.

```
VLL = 238e3; VLN = VLL/sqrt(3);
Srated = 50e6; Irated = Srated/(sqrt(3)*VLL);
Rtype = 'Air';

Xl = 1j*VLL^2/Srated;
XR = 377; Rl = abs(Xl)/XR;
Zsys = 9.29*exp(1j*86*pi/180);

M_max = 0.90; Rf = 1e-4;

for m = logspace(-3,0,10)
if contains( Rtype, 'Air', 'IgnoreCase', true )
    Radius = 4.2; Height = 11*2; % *feet
    Mutual_Min = Radius/Height; % *2 if mid-coil
    Mtf = Mutual_Min*m + (1-m)*M_max;
    Mft = Mutual_Min*(1-m) + m*M_max;
else % Iron-core
    Mtf = M_max; Mft = M_max;
end

T=[1 -Rf 0 0; ... % (7.1)
  -1 -m*(m*Xl+Rl) m*((m+(1-m)*Mtf)*Xl+Rl) 0; ...
   1  -m*Mft*Xl*(1-m) (1-m)*((1-m+m*Mft)*Xl+Rl) -1; ...
   0     0         Zsys      1]; % (7.14)
A = [0; 0; 0; VLN];
B = T\A;

fprintf( ['m = %5.1f%% -- If: %4.0f pu, ' ...
          'It: %7.3f pu, Vt: %4.1f%%\n'], ...
          100*m, abs(B(2))/Irated, ...
          abs(B(3))/Irated, 100*abs(B(4))/VLN );
end
```

TABLE VII
OUTPUT WHEN EXECUTING MATLAB PROGRAM

m (%)	If (pu)	It (pu)	Vt (%)
0.1	312	1.012	99.2
0.2	277	1.063	99.1
0.5	192	1.146	99.1
1.0	104	1.208	99.0
2.2	51	1.260	99.0
4.6	25	1.348	98.9
10.0	13	1.556	98.7
21.5	8	2.147	98.2
46.4	8	4.760	96.1
100.0	122	121.946	0.0

B. Mathcad Program for Faulted Reactor Model

The Mathcad program for the same air-core reactor turn faults is shown in Fig. 45.

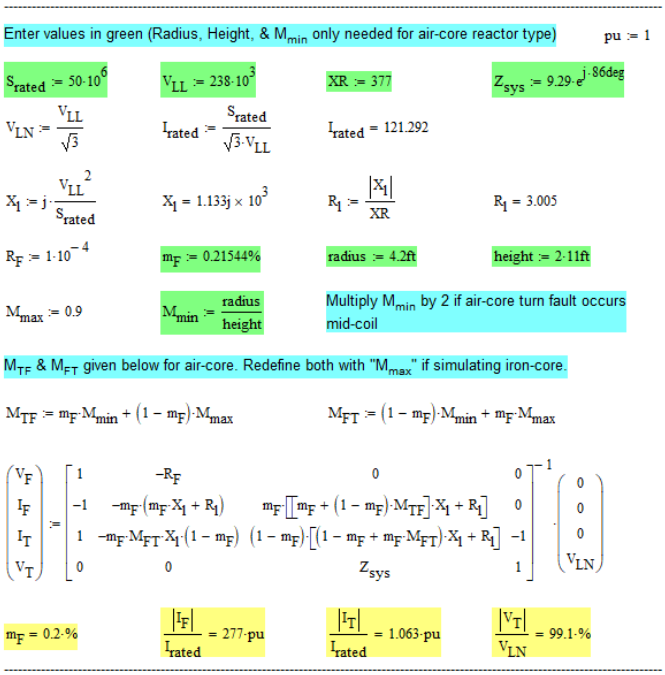

Fig. 45. Mathcad program for reactor turn fault model.

IX. APPENDIX B: AVISTA AIR-CORE SHUNT REACTOR PROTECTION SETTING SUMMARY

This section summarizes relevant system data from Table I to Table VIII and documents the relay settings (Table IX through Table XIV) deployed in the field. Details of setting descriptions and ranges can be found in [17]. The negative-sequence overcurrent elements shown in Table XI and Table XII are not required for a solidly grounded air-core reactor because the neutral overcurrent element provides equal sensitivity and operates quicker (Table V). They were configured only for field experience and verification of the guidance provided in this paper.

TABLE VIII
REACTOR BANK DATA RELEVANT FOR PROTECTION ELEMENT SETTINGS

Parameter	Value
Rated Current (I_{RATED})	121.3 A primary
PTR, CTR, and CTRN	2000, 240, and 80
I_{NOM_CTR} and I_{NOM_CTRN}	1 A secondary and 1 A secondary
Z_{REACT}	1,133 Ω primary or 139.9 Ω secondary

TABLE IX
ADAPTIVE SLOPE DIFFERENTIAL (87) ELEMENT SETTINGS

Setting	Value	Notes
O87P	0.30 pu	0.15 • (CTR • I_{NOM_CTR}) / I_{RATED} [15]
SLP1	35%	Slope that is secure for up to a 30% magnitude and 35° phase error
SLP2	50%	Slope that is secure for up to a 45% magnitude and 50° phase error

TABLE X
NEGATIVE-SEQUENCE DIRECTIONAL (32Q) ELEMENT SETTINGS

Setting	Value	Notes
Z1ANGS	89.85°	Arctangent of an X/R of 377 (τ = 1 s).
50FPS	0.05 A	6% • I_{RATED}/CTR = 0.03032 A. Configured to minimum allowable setting of 0.05 A.
50RPS	0.05 A	6% • I_{RATED}/CTR = 0.03032 A. Configured to minimum allowable setting of 0.05 A.
Z2FS	67.97 Ω	Z_{REACT} / 2
Z2RS	68.48 Ω	Z_{REACT} / 2 + 0.5 / I_{NOM_CTR}
A2S	0.02	I_2/I_1 > normal unbalance (Section IV.E.1)
ORDERS	Q	Using negative-sequence polarization because the reactor is not in an IBR plant (see Sections II.D and IV.F.3).

TABLE XI
DEFINITE-TIME OVERCURRENT (50Q) SETTINGS

Setting	Value	Notes
50SQ1P	0.40 A	80% of I_{RATED}
67SQ1TC	PSV25	Table XIII
67SQ1D	1.50 cycles	Fast element time delay (Table V)
50SQ2P	0.05 A	6% • I_{RATED} / CTR = 0.03032 A. Configured to minimum allowable setting of 0.05 A.
67SQ2TC	PSV25 AND NOT PCT25Q	Table XIII
67SQ2D	3.00 cycles	Sensitive element time delay (Table V)

TABLE XII
INVERSE-TIME OVERCURRENT (51) SETTINGS

Setting	Value	Notes
51O03	3I2SM	Operating current is 3I2 magnitude from terminal CTs
51P03	0.05054 A	51 element pickup is 10% • I_{RATED} / CTR = 0.05054 A
51C03	U2	Inverse curve (Table V)
51TD03	6	Time dial (Table V)
51TC03	PSV25	Table XIII

TABLE XIII
USER-PROGRAMMABLE PROTECTION SETTINGS
INCLUDING NEUTRAL OVERCURRENT (67N)

Setting	Value	Notes
PSV24	IASFM > 0.379 AND IBSFM > 0.379 AND ICSFM > 0.379	0.75 • I_{RATED} / CTR (Fig. 25). Add "…AND FREQOK AND (58.8 < FREQ AND FREQ < 61.2)" for line reactors (see Section IV.F.1).
PSV25	SF32Q AND PSV24	Forward and online
PCT25PU	0.25 cycles	NA
PCT25DO	1,800 cycles	30 seconds (Table V)
PCT25IN	SR32Q AND NOT PSV24	Disarm Zone 2
PCT26PU	1.50 cycles	Table V Row 1 (Zone 1)
PCT26DO	0 cycles	
PCT26IN	(IY1FM > 0.09097) AND PSV25	6% • I_{RATED} / CTRN

TABLE XIV
USER-PROGRAMMABLE FAULT-TYPE ID AND TARGET LED SETTINGS

Setting	Value	Notes
TRS	87R OR REF OR (PCT26Q OR 67SQ1T OR 67SQ2T OR 51T03) …	Output is TRIPS
PSV32	(PCT26Q OR 67SQ1T OR 67SQ2T OR 51T03) AND NOT (87R OR REF)	Turn fault (not phase or ground)
PCT32PU	0	NA
PCT32DO	1.5 cycles	Angle calculations window
PCT32IN	R_TRIG TRIPS	NA
PMV33	PCT32Q • (3I2SA – I1SA)	Fig. 29
PSV33	PMV33 < 0	–360° < PMV33 < 360°
PMV33	PSV33 • (PMV33 + 360) + NOT PSV33 • PMV33	0° ≤ PMV33 < 360°
PSV34	PSV32 AND PCT32Q AND (300 < PMV33 OR PMV33 <= 60)	PHASE A angle
PSV35	PSV32 AND PCT32Q AND (60 < PMV33 OR PMV33 <= 180)	PHASE B angle
PSV36	PSV32 AND PCT32Q AND (180 < PMV33 OR PMV33 <= 300)	PHASE C angle
T8_LED	TRIPS AND (87RA OR PSV34)	PHASE A LED
T9_LED	TRIPS AND (87RB OR PSV35)	PHASE B LED
T10_LED	TRIPS AND (87RC OR PSV36)	PHASE C LED
T11_LED	TRIPS AND PSV32	TURN LED
T12_LED	TRIPS AND REF	GROUND LED

X. References

[1] CIGRE WG B5.37 TB 546, "Protection, Monitoring and Control of Shunt Reactors," August 2013.

[2] IEEE Std C37.109-2006, *IEEE Guide for the Protection of Shunt Reactors.*

[3] E. Nashawati, N. Fischer, B. Le, and D. Taylor, "Impacts of Shunt Reactors on Transmission Line Protection," proceedings of the 38th Annual Western Protective Relay Conference, Spokane, WA, October 2011.

[4] Z. Gajić, B. Hillström, and F. Mekić, "HV Shunt Reactor Secrets for Protective Engineers," proceedings of the 30th Annual Western Protective Relay Conference, Spokane, WA, October 2003.

[5] D. Caverly, K. Pointner, R. Presta, P. Griebler, H. Reisinger, and M. Drive, "Air Core Reactors: Magnetic Clearances, Electrical Connection, and Grounding of their Supports," proceedings of the 53rd Annual Minnesota Power Systems Conference, St. Paul, MN, November 2017.

[6] P. Dopplmair, P. Venediger, K. Pointner, and T. Monni, "Evaluation and Implementation of HV Dry-Type Shunt Reactors into a 420 kV Transmission Grid," proceedings of SC A2 Power Transformers and Reactors, CIGRE, Paris, France, September 2022.

[7] P. I. Nyombi, Z. Zhang, and P. Mysore, "Implementation of a New Algorithm to Detect Turn-to-Turn Faults in Shunt Reactors and Identify the Faulted Phase," proceedings of the 74th Annual Conference for Protective Relay Engineers, Virtual Format, March 2021.

[8] IEEE Std C57.21-2021, *IEEE Standard for Requirements, Terminology, and Test Code for Shunt Reactors Rated Over 500 kVA*.

[9] IEC 60076-6, *Power Transformers – Part 6: Reactors*, 2007.

[10] RTDS Technologies Inc., *RTDS User's Manual*, Winnipeg, Canada, 2021.

[11] D. T. Paris and F. K. Hurd, *Basic Electromagnetic Theory*, McGraw-Hill, 1969.

[12] C. R. Paul, *Inductance: Loop and Partial,* Wiley-IEEE Press, 2009.

[13] H. Nie, X. Liu, Y. Wang, Y. Yao, Z. Gu, and C. Zhang, "Breaking Overvoltage of Dry-Type Air-Core Shunt Reactors and Its Cumulative Effect on the Interturn Insulation," *IEEE Access*, Vol. 7, 2019, pp. 550707–55720.

[14] B. Cook, C. Bolton, M. J. Thompson, and K. Garg, "SDG&E Relay Standards – Updating Tertiary Bus and Reactor Protection," proceedings of the 72nd Annual Conference for Protective Relay Engineers, College Station, TX, March 2019.

[15] R. Chowdhury, D. Finney, N. Fischer, and D. Taylor, "Determining CT Requirements for Generator and Transformer Protective Relays," proceedings of the 46th Annual Western Protective Relay Conference, Spokane, WA, October 2019.

[16] *SEL-400G Advanced Generator Protection System Instruction Manual*. Available: selinc.com.

[17] *SEL-487E Transformer Protection Relay Instruction Manual.* Available: selinc.com.

[18] R. Chowdhury, M. Alla, N. Fischer, and S. Samineni, "Restricted Earth Fault Protection in Low-Impedance Grounded Systems With Inverter-Based Resources," *IEEE Transactions on Power Delivery*, August 2022, pp. 1–8.

[19] G. Kobet, "Alarming Experience With Ungrounded Tertiary Bus Ground Detection," proceedings of the 48th Annual Western Protective Relay Conference, Virtual Format, October 2021.

[20] IEEE Std C37.234-2021, *IEEE Guide for Protective Relay Applications to Power System Buses*.

[21] IEEE Power and Energy Society, "Improved Generator Ground Fault Schemes," Technical Report PES-TR 82, September 2020.

[22] F. K. Basha and M. Thompson, "Practical EHV Reactor Protection," proceedings of the 66th Annual Conference for Protective Relay Engineers, College Station, TX, April 2013.

[23] B. Kasztenny, N. Fischer, and H. J. Altuve, "Negative-Sequence Differential Protection – Principles, Sensitivity, and Security," proceedings of the 41st Annual Western Protective Relay Conference, Spokane, WA, October 2014.

[24] R. Cole, R. Tuck, T. Solinsky, C. Sun, R. Chowdhury, A. Abd-Elkader, and B. Matta, "Bus Differential Protection Upgrade for a 1,500 MVA Nuclear Power Plant with Atypical Connections," proceedings of the 75th Annual Conference for Protective Relay Engineers, College Station, TX, March 2022.

[25] R. G. Bruce and A. Wright, "Remanent Flux in Current-Transformer Cores," *Proceedings of the Institution of Electrical Engineers*, Vol. 113, Issue 5, May 1966, pp. 915–920.

[26] H. Miller, J. Burger, and M. Thompson, "Automatic Reconfiguration of Zones for Three-Phase and Spare Banks," proceedings of the 36th Annual Western Protective Relay Conference, Spokane, WA, October 2009.

[27] F. Bassi, G. Ramundo, A. Di Tomasso, Y. Z. Korkmaz, and M. Donolo, "Case Study: How CT Saturation Due to Incorrect Point-on-Wave Switching Affects Shunt Reactor Differential Protection," proceedings of the 47th Annual Western Protective Relay Conference, Virtual Format, October 2020.

[28] R. Chowdhury, R. McDaniel, and N. Fischer, "Line Current Differential Protection in Systems With Inverter-Based Resources-Challenges and Solutions," proceedings of the 49th Annual Western Protective Relay Conference, Spokane, WA, October 2022.

[29] A. B. Dehkordi, R. Chowdhury, N. Fischer, and D. Finney, "Generator Protection Validation Testing Using a Real-Time Digital Simulator: Stator Winding Protection," proceedings of the 48th Western Protective Relay Conference, Virtual Format, October 2021.

[30] M. J. Thompson, "Percentage Restrained Differential, Percentage of What?" proceedings of the 37th Annual Western Protective Relay Conference, Spokane, WA, October 2010.

[31] K. H. Engelhardt, "EHV Line-Connected Shunt Reactor Protection Application and Experience," proceedings of the International Conference on Large High-Voltage Electric Systems, CIGRE, Paris, France, 1984.

[32] R. McDaniel and M. Thompson, "Impedance-Based Directional Elements – Why Have a Threshold Setting?" proceedings of the 48th Annual Western Protective Relay Conference, Spokane, WA, October 2021.

[33] M. H. Hesse and D. D. Wilson, "Near Resonant Coupling on EHV Circuits: II – Methods of Analysis," *IEEE Transactions on Power Apparatus and Systems*, Vol. PAS-87, No. 2, pp. 326–334, February 1968.

[34] CIGRE WG C4.307 TB 569, "Resonance and Ferroresonance in Power Networks," February 2014.

[35] R. Chowdhury and N. Fischer, "Transmission Line Protection for Systems With Inverter-Based Resources - Part I: Problems," in *IEEE Transactions on Power Delivery*, Vol. 36, No. 4, August 2021, pp. 2416–2425, doi: 10.1109/TPWRD.2020.3019990.

[36] S. Das, T. Sidhu, M. Zadeh, and Z. Zhang, "A Novel Method for Turn to Turn Fault Detection in Shunt Reactors," proceedings of the 70th Annual Conference for Protective Relay Engineers, College Station, TX, April 2017.

[37] B. Kasztenny, M. J. Thompson, and D. Taylor, "Time-Domain Elements Optimize the Security and Performance of Transformer Protection," proceedings of the 71st Annual Conference for Protective Relay Engineers, College Station, TX, March 2018.

[38] IEEE Std C37.015-2017, *IEEE Guide for the Application of Shunt Reactor Switching*.

[39] F. W. Grover, "Inductance Calculations," Dover Publications, October 2009.

[40] D. C. Hanselman, *Brushless Permanent-Magnet Motor Design*, McGraw-Hill, Inc. New York, NY, 1994, pp. 13–38.

XI. Biographies

Ritwik Chowdhury received his BS degree in engineering from the University of British Columbia and his MS degree in engineering from the University of Toronto. He joined Schweitzer Engineering Laboratories, Inc. (SEL) in 2012, where he is presently a senior engineer in research and development. Ritwik holds 9 patents and has helped author 25 technical papers. He was recognized as an exceptional reviewer for *IEEE Transactions on Power Delivery* for 2019 and 2021. He is the vice chair of the Protection and Control Practices Subcommittee (I-SC) of the IEEE Power System Relaying and Control (PSRC) Committee, the chair of two IEEE Standards Working Groups, and the recipient of the 2021 PSRC Outstanding Young Engineer Award. Ritwik is a senior member of IEEE, a member of CIGRE, and a registered professional engineer in the province of Ontario.

Normann Fischer received a Higher Diploma in Technology, with honors, from Technikon Witwatersrand, Johannesburg, South Africa, in 1988; a BSEE, with honors, from the University of Cape Town in 1993; an MSEE from the University of Idaho in 2005; and a PhD from the University of Idaho in 2014. He joined Eskom as a protection technician in 1984 and was a senior design engineer in the Eskom protection design department for three years. He then joined IST Energy as a senior design engineer in 1996. In 1999, Normann joined Schweitzer Engineering Laboratories, Inc., (SEL) where he is currently a distinguished engineer in research and development. He was a registered professional engineer in South Africa and a member of the South African Institute of Electrical Engineers. He is currently a senior member of IEEE and a member of the American Society for Engineering Education (ASEE). Normann has authored over 60 technical and 10 transaction papers and holds over 20 patents related to electrical engineering and power system protection.

Douglas Taylor received his BSEE and MSEE degrees from the University of Idaho in 2007 and 2009. He joined Schweitzer Engineering Laboratories, Inc. (SEL) in 2009 and worked as a protection engineer and a research engineer in the research and development division. In 2019, Doug joined the system protection group at Avista Utilities and currently serves as a senior protection engineer. He is a registered professional engineer in the state of Washington and a member of the WPRC planning committee. Doug's main interests are power system protection and power system analysis. He holds 3 patents and has coauthored over 20 technical papers in the area of power system protection.

David Caverly received his Bachelor of Applied Science degree in engineering science (electrical engineering) from the University of Toronto in 1978. Following his graduation, he joined Trench Limited in the research and development department, specializing in electric coil products. His current role is vice president of business development for coil products, and he focuses on coil business development and application support for customers in the field of air-core reactors. David is a member of IEEE and CIGRE and participates in the IEEE Transformers Committee, IEEE Switchgear Committee, and the IEEE Power Systems Relaying Committee.

Ali B. Dehkordi received BSc and MSc degrees in electrical engineering from Sharif University of Technology, Tehran, Iran, and a PhD degree from the University of Manitoba, Canada, in 1999, 2002, and 2010, respectively. Between 1998 and 2002, he worked on various industrial projects that included substation and transformer maintenance as well as power quality projects. His research interests involve modeling power system and power electronic components, specifically electric machines for electromagnetic transient programs and real-time digital simulation (RTDS), the area that he has been working on for over 18 years. Dr. Dehkordi is a recipient of the Dennis Woodford Prize for "the most outstanding graduate thesis dealing with power system modeling and simulation." He is currently employed by RTDS Technologies Inc., located in Winnipeg, Canada. He is a senior member of IEEE.